Received: 20 January 2020 | Revised: 28 May 2020 | Accepted: 9 June 2020

DOI: 10.1111/all.14481

ORIGINAL ARTICLE

Allergen-Specific Immunotherapy and Biologics

Allergy EUROPEAN JOURNAL OF ALLERGY AND CLINICAL IMMUNOLOGY EAACI WILEY

Laser-facilitated epicutaneous immunotherapy with hypoallergenic beta-glucan neoglycoconjugates suppresses lung inflammation and avoids local side effects in a mouse model of allergic asthma

Evgeniia Korotchenko[1] | Viktoria Schießl[1] | Sandra Scheiblhofer[1] | Mario Schubert[1] | Elfriede Dall[1] | Isabella A. Joubert[1] | Helen Strandt[1] | Theresa Neuper[1] | Muamera Sarajlic[1] | Renate Bauer[1] | Mark Geppert[1] | David Joedicke[2] | Sabrina Wildner[1] | Susanne Schaller[2] | Stephan Winkler[2] | Gabriele Gadermaier[1] | Jutta Horejs-Hoeck[1] | Richard Weiss[1]

[1]Department of Biosciences, University of Salzburg, Salzburg, Austria

[2]Research and Development, University of Applied Biosciences Upper Austria, Hagenberg, Austria

Correspondence
Richard Weiss, Department of Biosciences, University of Salzburg, Salzburg, Austria.
Email: Richard.Weiss@sbg.ac.at

Funding information
Austrian Science Fund, Grant/Award Number: W 1213

Abstract

Background: Allergen-specific immunotherapy via the skin targets a tissue rich in antigen-presenting cells, but can be associated with local and systemic side effects. Allergen-polysaccharide neoglycogonjugates increase immunization efficacy by targeting and activating dendritic cells via C-type lectin receptors and reduce side effects.

Objective: We investigated the immunogenicity, allergenicity, and therapeutic efficacy of laminarin-ovalbumin neoglycoconjugates (LamOVA).

Methods: The biological activity of LamOVA was characterized in vitro using bone marrow-derived dendritic cells. Immunogenicity and therapeutic efficacy were analyzed in BALB/c mice. Epicutaneous immunotherapy (EPIT) was performed using fractional infrared laser ablation to generate micropores in the skin, and the effects of LamOVA on blocking IgG, IgE, cellular composition of BAL, lung, and spleen, lung function, and T-cell polarization were assessed.

Results: Conjugation of laminarin to ovalbumin reduced its IgE binding capacity fivefold and increased its immunogenicity threefold in terms of IgG generation. EPIT with LamOVA induced significantly higher IgG levels than OVA, matching the levels induced by s.c. injection of OVA/alum (SCIT). EPIT was equally effective as SCIT in terms of blocking IgG induction and suppression of lung inflammation and airway hyperresponsiveness, but SCIT was associated with higher levels of therapy-induced

Abbreviations: EPIT, epicutaneous immunotherapy; LamOVA, laminarin-ovalbumin conjugates; OVA, ovalbumin; PBS, phosphate buffered saline; Penh, resistance and compliance data are shown as area under the curve (AUC) of a methacholine challenge dose response curve; SCIT, subcutaneous immunotherapy.

This is an open access article under the terms of the Creative Commons Attribution License, which permits use, distribution and reproduction in any medium, provided the original work is properly cited.
© 2020 The Authors. *Allergy* published by European Academy of *Allergy* and Clinical Immunology and John Wiley & Sons Ltd

IgE and TH2 cytokines. EPIT with LamOVA induced significantly lower local skin reactions during therapy compared to unconjugated OVA.

Conclusion: Conjugation of ovalbumin to laminarin increased its immunogenicity while at the same time reducing local side effects. LamOVA EPIT via laser-generated micropores is safe and equally effective compared to SCIT with alum, without the need for adjuvant.

KEYWORDS

dendritic cell targeting, epicutaneous immunotherapy, glycoconjugates, laser, skin vaccination

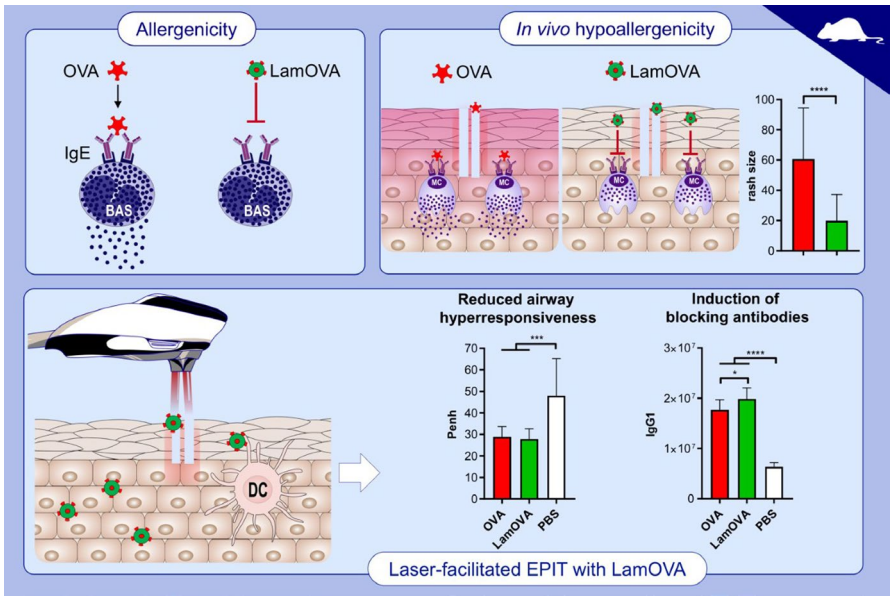

GRAPHICAL ABSTRACT

Epicutaneous immunotherapy (EPIT) targets a tissue rich in antigen-presenting cells. Laser-facilitated EPIT combines controlled and efficient barrier disruption with a laser-induced adjuvant effect. However, application of native allergens to the skin can induce unwanted side effects. Coupling the β-glucan laminarin to allergens can markedly reduce their IgE binding capacity. β-glucan neoglycoconjugates efficiently target dendritic cells via the C-type lectin receptor dectin-1, boosting their immunogenicity. In a mouse model of allergic asthma, laminarin-ovalbumin conjugates (LamOVA) diminished local side effects in vivo, while inducing higher levels of blocking IgG compared with uncoupled OVA. EPIT with LamOVA was equally efficient in improving lung functions compared to classical SCIT.

1 | INTRODUCTION

Epicutaneous allergen-specific immunotherapy (EPIT) has been introduced almost 100 years ago and only recently revisited.[1] Current studies show that EPIT can lead to a potent reduction of allergic symptoms and that the efficacy of the therapy is dependent on the allergen dose and the pretreatment of the skin. However, depending on the degree of barrier disruption, epicutaneous application of allergen can induce local and even systemic side effects in some individuals.[2] Alternatively, therapy has been performed by application of occlusive patches to intact skin leading to epicutaneous absorption due to maceration.[3] The major pitfall of this method is the inefficient uptake, requiring numerous applications of high doses.[4]

Due to the high number of antigen-presenting cells (APCs) in the epidermis and dermis, skin-based immunization often requires smaller amounts of antigen to induce immune responses compared to subcutaneous (s.c.) or intramuscular injections.[5] APCs express a large variety of pattern-recognition receptors (PRRs) determining their main function, that is, sensing of pathogens and induction of immune reactions.[6] One group of PRRs are C-type lectin receptors (CTLs), which bind to carbohydrates in a calcium-dependent manner. Together with other receptors, stimulation of CTLs determines the activation status of dendritic cells (DCs) and subsequent T-cell polarization.[7] Therefore, the use of protein neoglycoconjugates for immunizations can increase vaccine potency.

As a prominent member of the CTL family, Dectin-1 is functionally equivalent in mice and humans.[8] It recognizes β-glucans and some proteins such as tropomyosin,[9] and upon ligand binding activates innate

immune responses. Murine Dectin-1 is expressed on macrophages, neutrophils, and dermal DCs.[10] In humans, Dectin-1 is not restricted to cells of the myeloid lineage but can also be found on epithelial cells,[8,11,12] keratinocytes,[13] B cells, and subpopulations of T cells.[8] As Dectin-1 is expressed on dermal DCs, its use as a vaccination platform for targeted skin vaccination is highly promising. Here, we used 4-5 kDa laminarin/ovalbumin (LamOVA) conjugates for allergen-specific immunotherapy (AIT). Laminarin has strong immunostimulatory properties and has been employed in tumor therapy for activation of the innate immune system.[14] Moreover, polysaccharides can mask epitopes on allergens preventing IgE cross-linking on mast cells and histamine release, decreasing the risk of side effects.[15]

Skin has a protective function, and its outermost layer, the stratum corneum, represents a tight barrier that has to be overcome for antigen delivery. We use infrared laser to form micropores in the upper layers of the skin.[16] Besides facilitating vaccine penetration, the local tissue damage caused by laser treatment attracts large numbers of APCs and creates a pro-inflammatory milieu, thereby acting as a physical adjuvant for skin vaccinations.[17]

In our current work, we evaluated the immunostimulatory capacity of LamOVA conjugates and their efficacy in a preventive and therapeutic BALB/c mouse model of allergic lung inflammation. Laser-facilitated EPIT with LamOVA significantly reduced airway hyperresponsiveness and local side effects in vivo.

2 | MATERIALS AND METHODS

A more detailed version of materials and methods and a complete list of used antibodies and their dilutions (Table S1) can be found in the Supplementary Materials.

2.1 | Generation and analysis of allergen-carbohydrate neoglycoconjugates

Laminarin from laminaria digitata (Sigma, L9634, batch SLBP4829V) was dialyzed with a cut-off of 2 kDa to remove low molecular weight impurities and partially oxidized with sodium (meta)periodate (Sigma).[15] Briefly, 400 mg of laminarin were reacted with 95.2 mg sodium (meta)periodate for 1 hour at RT followed by dialysis against 50 mM phosphate buffer, pH 7. Laminarin and its oxidized variant were analyzed by two-dimensional NMR spectroscopy. Oxidized laminarin was coupled to endotoxin-free ovalbumin (OVA, EndoFit™ Ovalbumin, InvivoGen) using 2-step reductive amination with 50 mM sodium cyanoborohydride ($NaCNBH_3$) and 10 mM sodium borohydride ($NaBH_4$) as previously described.[15] Resulting neoglycoconjugates were separated by size-exclusion chromatography on a HiPrep 26/100 Sephacryl® S-200 HR column (GE Healthcare Life Sciences), and fractions were analyzed by 10% SDS-PAGE. Fractions containing high molecular weight (>70 kDa) laminarin-ovalbumin conjugates (LamOVA) were used for further experiments.

Carbohydrate concentration in conjugates was estimated using anthrone method [18] and OVA concentration was determined by amino acid analysis.[19] The hydrodynamic radius of conjugates was analyzed by dynamic light scattering using a Zetasizer Nano ZS with a DTS1070 capillary cell (Malvern Instruments).

Biological activity of laminarin in LamOVA conjugates was analyzed by ELISA using a soluble murine Fc-Dectin-1a receptor (InvivoGen) and by Microscale Thermophoresis (MST) using a Monolith NT.115 RED instrument (Nanotemper, Munich, Germany). Hypoallergenicity was analyzed in vitro as a measure of rat basophil leukemia cell (RBL-2H3) activation by β-hexosaminidase release assay.[15]

2.2 | Uptake and activation analysis using bone marrow-derived dendritic cells

Bone marrow-derived dendritic cells (BMDCs) were harvested from mouse femur and tibia and incubated with either 20 ng/mL murine GM-CSF (Immunotools, Cat. Nr 12343125) or 200 ng/mL human Flt3-L (AcroBiosystems, Cat. Nr FLL-H55H7) as described[20,21] with minor changes.

LamOVA effects on CD86 and Dectin-1 expression on CD11c + Flt3-L—generated DCs (FL-DCs) and on CD11c + $MHCII^{high}$ $CD11b^{int}$ GM-CSF—derived DCs (GM-DCs) were assessed. Activation of OVA-specific naïve DO11.10 T cells was analyzed in co-culture assays. BMDC activation, T-cell proliferation, and uptake were assessed by flow cytometry as described in Supplementary Materials. Cytokine concentration in supernatants was analyzed by LEGENDplex assay (Biolegend) using the 13-plex mouse inflammation panel and the 13-plex mouse proinflammatory chemokine panel according to the manufacturer's instructions.

2.3 | Animal experiments

Female BALB/c mice aged 6-8 weeks were obtained from Janvier (Le Genest-Saint-Isle, France) and maintained at the animal facility of the University of Salzburg in an SPF environment according to local guidelines. All animal experiments were conducted in compliance with EU Directive 2010/63/EU and have been approved by the Austrian Ministry of Education, Science and Research, permit number BMBWF-66.012/0006-V/3b/2018. Blood samples were drawn on days 27, 35, 55 (prevention) and 16 and 86 (therapy) by puncture of v. saphena.

To study immunogenicity of the conjugates, mice (n = 6) were immunized three times with 20 μg of OVA, LamOVA conjugates (20 μg OVA coupled to 49 μg laminarin), a mixture of equivalent amounts of OVA + laminarin, or laminarin and PBS (sham controls). The antigens were applied to laser-microporated skin on days 1, 15, and 29. Microporation was performed using a PLEASE® professional infrared laser device (Pantec Biosolutions, Ruggell, Liechtenstein) with a total fluence of 8.3 J/cm^2 as previously

described.[15] After the third immunization, mice were sensitized two times in a ten-day interval (days 36 and 46) by i.p. injections of 1 μg EndoFit™ OVA adsorbed to 50% (v/v) alum (Alu-Gel-S, Serva) in endotoxin-free PBS. To induce lung inflammation, animals were challenged by exposure to aerosolized grade V OVA from Sigma (A5503) that has been purified from endotoxin using Triton-X114 method[22] (10 mg/mL in 0.9% NaCl, LPS <0.39 pg per 1 μg OVA), for 30 minutes on days 53-55 using a Pariboy SX jet nebulizer with a Pari LL nebulizer head (Pari GmbH).

To study therapeutic efficacy, animals (n = 12) were sensitized by two i.p. injections with 10 μg of EndoFit™ OVA/alum on days 1 and 8. On day 15, mice were challenged intranasally with 10 μg of EndoFit™ OVA in 40 μL PBS, under isoflurane anesthesia. One day after the challenge, lung function and specific serum IgE were analyzed to confirm that all animals in the treatment groups had an asthma-like phenotype and OVA-specific IgE. Eight therapeutic immunizations were performed between days 18 and 67 in weekly intervals. Mice were treated with LamOVA conjugates, OVA, laminarin, or PBS. 35 μg of OVA and/or 86 μg of laminarin equivalents were applied on 1 cm^2 of laser-microporated skin. As a positive control, s.c. injections with 35 μg EndoFit™ OVA/alum were performed. On days 84-86, mice were challenged with OVA aerosol.

2.4 | Analysis of local side effects

For analysis of erythema severity, mice were photographed on days 47 or 54 with a SONY ILCE-7M2 camera, 28-70 mm zoom lens with a constant source of light using.JPG format. MATLAB R2019a was used for analysis. Briefly, the area of laser microporation (region of interest, ROI) was defined by an investigator blinded to the treatment. Based on the gray value of the selected ROI, a threshold was manually selected, to define the erythema that was darker than healthy skin. Erythema size and mean blob size were calculated from the selected ROI. Erythema size is calculated as the ratio of pixels above the chosen threshold to the number of pixels inside the ROI. A blob is defined as the sum of directly connected pixels of the segmented erythema. The mean value of the five biggest blobs was evaluated.

2.5 | Lung function analysis

The day after the aerosol challenge, lung function was analyzed by whole-body plethysmography (WBP) using a Buxco 6-chamber unrestrained WBP system (Data Sciences International). The next day, lung resistance/compliance measurement was performed using a FinePointe Series Resistance and Compliance (RC) site (Data Sciences International). Bronchoalveolar lavage fluid (BALF) was collected, and its cellular composition was analyzed by flow cytometry staining for Siglec F, CD45, CD4, CD8, CD19, and Ly6G/Ly6C (Gr-1).

2.6 | Lung digestion

Lung tissue was digested, and total leukocytes were separated using biotinylated CD45 and BD™ IMag Streptavidin Particles (BD Biosciences). Cells were stained for CD11b, CD24, CD4, CD45, Ly6G/Ly6C (Gr-1), MHC-II, and Siglec F and analyzed by flow cytometry.

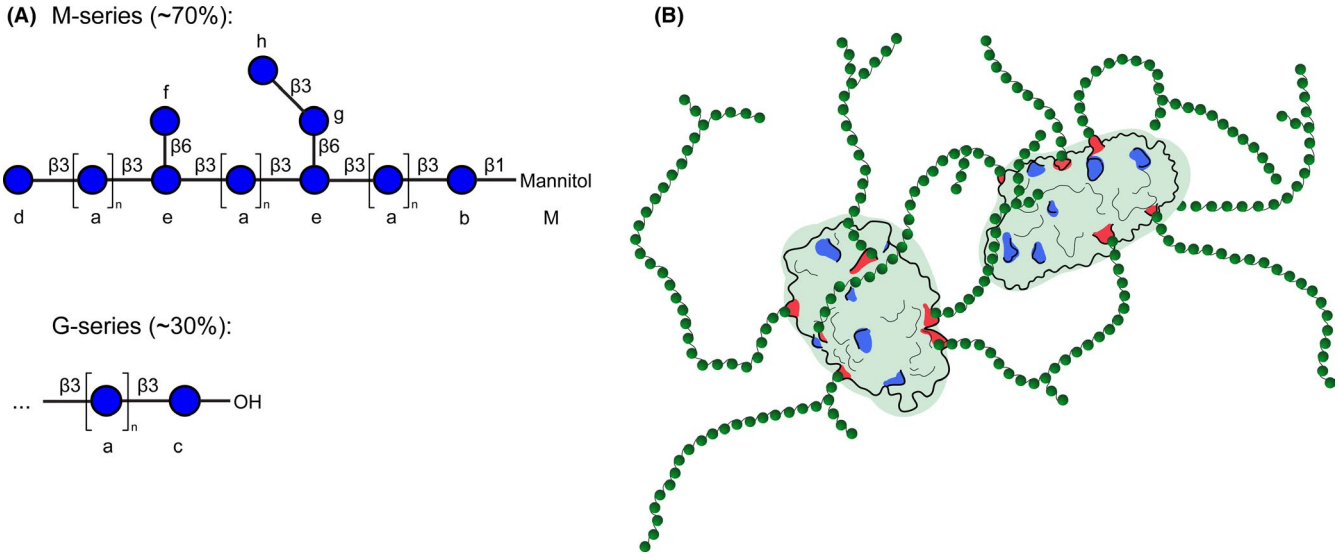

FIGURE 1 (A) Structure of laminarin as determined by NMR. Glucose residues that are distinguishable by NMR spectroscopy are labeled with small letters a to h and the mannitol is abbreviated with M. β1-3 and β1-6 glycosidic bonds are indicated as β3 and β6, respectively. (B) Schematic model depicting OVA (PDB: 1OVA) with 6 covalently linked chains of laminarin. The six lysine residues that have a fractional accessible surface area >0.5 at least in one of the four structures in the asymmetric unit of the crystal structure are shown in red, the other lysines in blue. A potential cross-linking of two OVA molecules is shown

2.7 | Analysis of OVA-specific serum IgG/IgE and cell-bound IgE

OVA-specific IgG isotypes in sera were analyzed by direct ELISA. OVA-specific serum IgE was measured using a rat basophil leukemia cell (RBL-2H3) assay. Briefly, cells were incubated for 2 hours with mouse sera diluted 1:150 in medium, followed by three washing steps and 1 hour stimulation with 0.3 μg/mL EndoFit™ OVA. β-hexosaminidase levels in supernatants were measured and degranulation was calculated as percentage of total lysis from control wells lysed with Triton X-100.

Cell-bound IgE was analyzed ex vivo by basophil activation test from whole blood drawn one day after the second aerosol challenge. Cells were stimulated in the presence or absence of autologous serum with 2 ng/mL OVA for 2 hours at 37°C, 5% CO_2, 95% humidity. After the incubation, cells were stained for IgE, CD4, CD19, and CD200R and analyzed by flow cytometry on a FACS Canto II flow cytometer (BD Biosciences).

2.8 | Lymphocyte restimulation

Spleens were harvested for T-cell restimulation with OVA. After erythrocyte lysis in Ammonium-Chloride-Potassium (ACK) lysing buffer, splenocytes were resuspended in T-cell medium (RPMI-1640, 10% FCS, 25 mM Hepes, 2 mM L-Glu, 100 μg/mL streptomycin, 100 U/mL penicillin) and 0.6×10^6 cells/well were stimulated with 0.1 mg/mL EndoFit™ OVA and incubated for 3 days at 37°C, 5% CO_2. Supernatants were harvested and analyzed by LEGENDplex immunoassay using the mouse T helper 13-plex cytokine panel. Cells were stained for CD4, CD25, CD44, FoxP3, GATA3 and analyzed by flow cytometry on a Cytoflex S flow cytometer (Beckman Coulter).

2.9 | Statistical analysis

Data were statistically analyzed using GraphPad Prism 7 using one-way ANOVA with Tukey's post hoc test unless otherwise specified. *P*-values are shown as: $^*P \leq .05$, $^{**}P \leq .01$, $^{***}P \leq .001$, $^{****}P \leq .0001$.

3 | RESULTS

3.1 | Generation of laminarin-OVA conjugates

NMR analysis of the used laminarin batch (SLBP4829V) indicated approx. 70% M-series (terminated with 1-linked d-mannitol) and 30% G-series (containing only glucose) in the fresh and also in the dialyzed laminarin sample (Figure 1A and Figures S1 and S2). Approx. 1.5 branch sites per molecule were observed. These findings are in agreement with previously published data (Table S2).[23,24] Previous studies have found laminarin from the same supplier to be in the size range of 4-5 kD[25] which is in line with data from Read et al[24] and also fits to our NMR data. For all further calculations, we thus estimated a MW of 4.5kD for the used laminarin batch. Upon treatment with periodate, all the signals of the mannitol (Figure 1A, Figures S1 and S2, unit M) and the unprotected glucose moieties at the reducing end (unit c) disappeared and the terminal glucose moieties (units d, f and h) decreased in their signal intensity, indicating successful oxidation. These were also the expected sites for periodate oxidation, indicated in red in Figure S2, as they contain accessible and neighboring OH groups that can react with periodate to generate reactive aldehyde groups. This is in agreement with the study by Read et al, who showed by mass spectrometry that only the terminal Glc moieties of both, the main chain and the side chains are oxidized.[24]

Neoglycoconjugates were generated by coupling of oxidized laminarin to EndoFit™ OVA by reductive amination. Size-exclusion

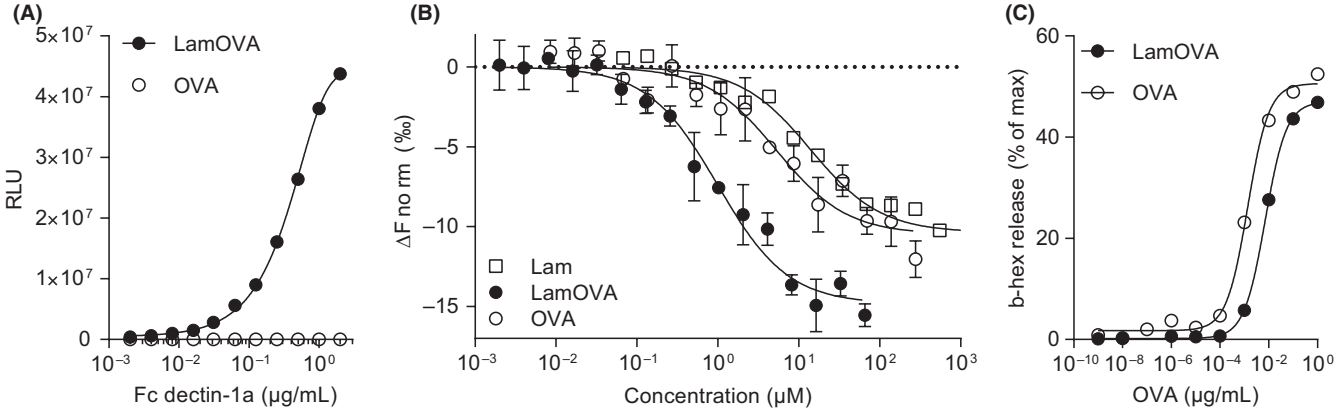

FIGURE 2 Binding of soluble Dectin-1a receptor (fused to IgG-Fc) to plate-bound LamOVA or OVA (A) or soluble LamOVA, OVA, and laminarin (B). Data are shown as relative light units (RLU) of a luminometric ELISA (A) or as changes in normalized fluorescence (ΔFnorm) of MST measurements (mean ± SD of three independent binding experiments). (C) Stimulation of IgE-loaded RBL cells with LamOVA or OVA. Basophil IgE-mediated degranulation is presented as percentage of total beta-hexosaminidase (b-hex) release

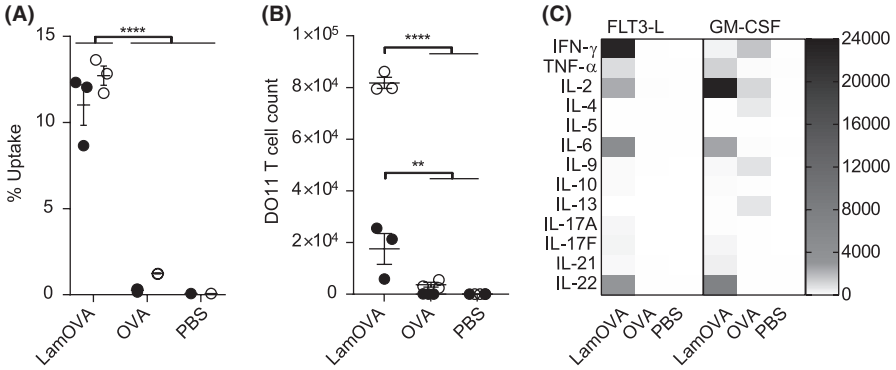

FIGURE 3 (A) Uptake of pHrodo-labeled OVA or LamOVA conjugates by GM-BMDCs (white circles) and FL-BMDCs (black dots) was analyzed by flow cytometry after 24 hours. (B) Proliferation of OVA-specific DO11.10 T cells after 5 days co-culture with BMDCs and OVA or LamOVA. Data are shown as number of live, proliferating DO11.10 cells. (C) Cytokine concentration in BMDC-T cell co-culture supernatants in pg/mL. Means ± SEM and individual technical replicates (n = 3) are shown. Data were statistically analyzed by two-way ANOVA followed by Tukey's post hoc test

chromatography (Figure S3A) was used to separate neoglycoconjugates by size, followed by SDS-PAGE of the fractions (Figure S3B). Based on visual analysis, fractions migrating above 70 kDa were pooled (LamOVA) and further analyzed.

To determine OVA concentration in conjugates, amino acid analysis was used (Figure S3C), as common methods of protein quantification such as UV absorption, Bradford assay, or BCA assay are all affected by the carbohydrate moiety. Additionally, this method allows estimating the amount of lysine residues which participated in reductive amination. For LamOVA, an average of 6 out of 20 lysines was coupled to laminarin. This is in line with in silico prediction using the VADAR server,[26] showing that 6 lysines have a fractional accessible surface area (ASA) >0.5 at least in one of the four structures in the asymmetric unit of the crystal structure 1OVA.pdb. These are K39, K78, K105, K135, K236, and K292 (shown in red in Figure 1B), which are therefore most likely involved in laminarin coupling. This coupling rate of 6 molecules laminarin to 1 molecule of OVA corresponds to a carbohydrate to protein ratio of 0.6 (w/w). This was supported by SDS-PAGE where the majority of the conjugates migrated between 70 and 130 kD. As laminarin does not bind SDS, the net charge-to-mass ratio of the protein-SDS complex is reduced, resulting in an overestimation of its molecular weight. Thus, we surmise that the majority of LamOVA consists of monomeric OVA with an average of 6 molecules of laminarin covalently linked (Figure 1B). An additional faint band migrating above 180 kD in the SDS-PAGE in the high molecular weight fractions 26-29 probably corresponds to conjugates containing more than one molecule of OVA due to cross-linking via laminarin. As shown by dynamic light scattering (Figure S3D), conjugates were homogeneous in size and had a diameter of 8.27 ± 0.75 nm, which also supports the prevalence of monomeric rather than cross-linked LamOVA conjugates (given a hydrodynamic radius of ~3 nm for monomeric OVA).

Estimation of carbohydrate content in LamOVA by the anthrone method indicated a higher carbohydrate/protein ratio of 2.5 (w/w), which can be explained by the inaccuracy of the method, the presence of noncovalently attached laminarin and/or free laminarin not completely removed by SEC. Nevertheless, we calculated with a carbohydrate/protein ratio of 2.5 when using laminarin controls in the subsequent experiments to avoid any potential underestimation of the amount of laminarin in the conjugates.

3.2 | Laminarin is biologically active after conjugation

To ensure that the structure of laminarin was not destroyed during mild periodate oxidation and that the polysaccharide remained biologically active after coupling, binding to Dectin-1 was assessed by ELISA and MST. As shown in Figure 2A, plate-bound LamOVA was recognized by Dectin-1, whereas no binding to unconjugated OVA was observed. To verify that the observed differences were not due to relative coating efficiencies of OVA and LamOVA or unspecific binding of LamOVA due to denaturation and aggregation, we confirmed these results in solution using MST (Figure 2B) and included an unspecific soluble receptor (TLR5) as a control (Figure S4). Using Hill fit model for multiple binding, the apparent dissociation constant (Kd_{app}) for binding of LamOVA and 4.5 kD laminarin to Dectin-1 was 0.99 ± 0.17 μM vs 13.98 ± 3.03 μM (calculating with a carbohydrate to protein ratio of 0.6). Even considering additional noncovalently linked laminarin in the conjugate preparation (carbohydrate to protein ratio of 2.5 based on anthrone method), the resulting Kd_{app} value of 4.22 ± 0.72 μM was still threefold lower compared with 4.5 kD laminarin. These data indicate that LamOVA conjugates bind Dectin-1 in solution with a threefold to 13-fold higher affinity compared to unconjugated laminarin. Similar values were obtained for oxidized laminarin (data not shown). Based on the OVA concentration in the conjugates, coupling of OVA to laminarin increased its affinity for Dectin-1 30-fold compared to soluble OVA (0.17 ± 0.03 μM vs 5.33 ± 1.75 μM). Although LamOVA showed a higher binding affinity for TLR5 than laminarin (6 ± 2 μM vs 74 ± 46 μM; Figure S4), this was still sixfold lower compared with its affinity for Dectin-1, confirming the specificity. The partial

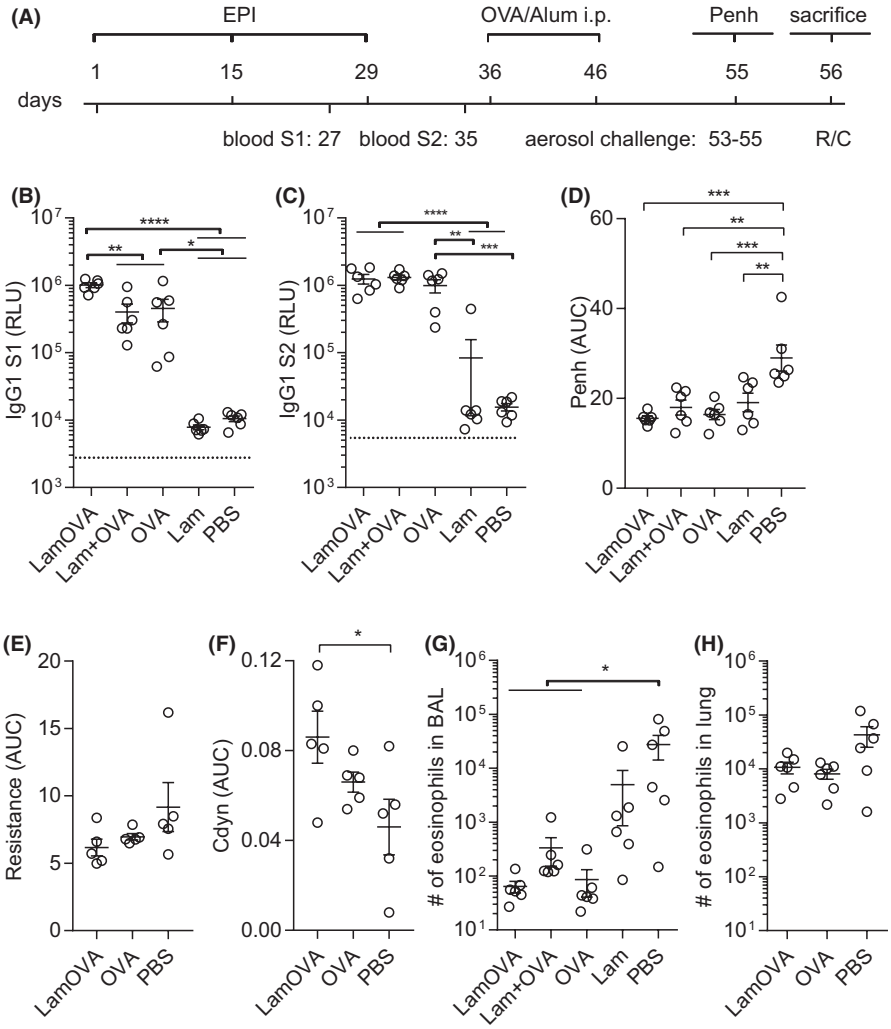

FIGURE 4 Prophylactic epicutaneous immunization via laser-generated micropores (EPI). (A) Mice were immunized 3 times with LamOVA, OVA, a mix of OVA with laminarin (Lam + OVA), laminarin (Lam) or PBS followed by i.p. sensitization and aerosol challenge. Numbers indicate days. OVA-specific serum IgG1 was measured after two (B, S1) or three (C, S2) immunizations at a serum dilution of 1:10 000. Data are shown as relative light units (RLU) of a luminometric ELISA (n = 6). Background is indicated by dotted line. Airway hyperresponsiveness was assessed by WBP (D, n = 6), as well as resistance (E, n = 5) and compliance (F, n = 5) measurements. Penh, resistance, and compliance data are shown as area under the curve (AUC) of a methacholine challenge dose-response curve. Numbers of eosinophils in BAL (G, n = 6) or collagenase-digested lung preparations (H, n = 6) were analyzed by flow cytometry

binding of LamOVA to TLR-5 was probably due to the OVA moiety of the conjugates, as unconjugated OVA showed the highest affinity for TLR-5 (0.8 ± 0.3 μM).

3.3 | LamOVA conjugates activate RBL cells to a fivefold lesser extent than unmodified OVA

Hypoallergenicity is a prerequisite for AIT via the skin, as administration of native allergen to barrier disrupted skin has been shown to induce local or even systemic side effects.[2] We hypothesized that laminarin polysaccharide chains (6 kDa) would mask IgE epitopes of OVA and prevent mast cell and basophil degranulation in vivo. To prove that conjugates were less allergenic than unconjugated OVA, rat basophil leukemia (RBL) cells were incubated with sera of highly sensitized mice and stimulated with LamOVA or OVA. Beta-hexosaminidase secretion after antigen stimulation is a measure of IgE cross-linking. As shown in Figure 2C, a fivefold higher dose of LamOVA was required to activate IgE-loaded RBL cells compared with OVA thus confirming hypoallergenicity of LamOVA.

3.4 | Laminarin conjugation to OVA facilitates uptake by BMDCs and induces their activation

Bone marrow cells were incubated with either hFLT3-L (FL) or mGM-CSF (GM) to generate BMDCs. Uptake of pHrodo-labeled LamOVA was significantly enhanced compared to pHrodo-OVA in both FL-BMDCs and GM-BMDCs (Figure 3A). LamOVA significantly activated BMDCs in a dose-dependent manner, whereas unconjugated OVA and laminarin (used at doses equivalent to those present in LamOVA) did not induce CD86 expression even at the highest doses. GM-BMDCs showed a higher base-line expression of CD86 and responded more strongly to positive control stimulus LPS than to LamOVA (Figure S5A). In contrast, FL-BMDCs had a more naïve phenotype and LamOVA induced an equivalent upregulation of CD86 compared with LPS (Figure S5B). In both cell types, LamOVA induced significantly higher CD86 expression than OVA, laminarin, and PBS stimulation (Figure S5A and B). LamOVA and laminarin stimulation significantly downregulated Dectin-1 surface expression in GM-BMDCs and FL-BMDCs (Figure S5C and D), indicating binding of the beta-glucan to its receptor. Interestingly, LPS activation also induced downregulation of Dectin-1, which has already been observed in macrophages.[27]

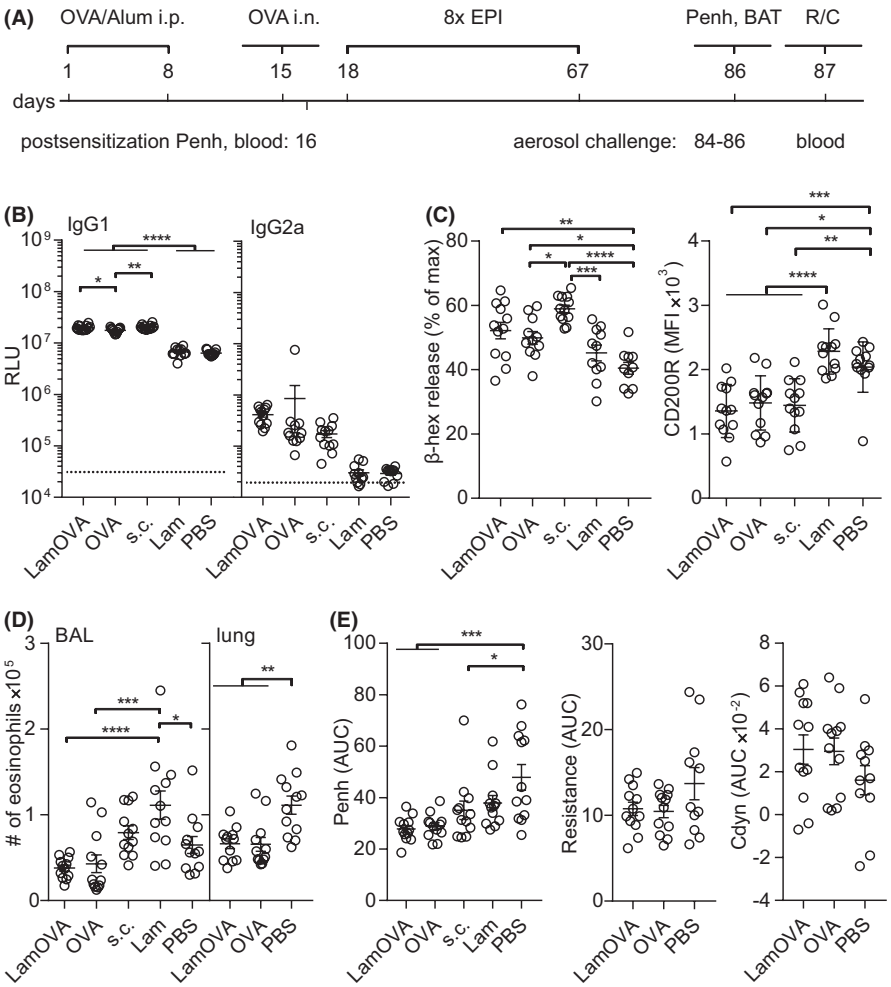

FIGURE 5 Therapeutic epicutaneous immunization via laser-generated micropores (EPIT). (A) Mice were sensitized by two i.p. injections with OVA/alum and an intranasal challenge. After 8 treatments, either epicutaneously (LamOVA, OVA) or subcutaneously with OVA/alum (s.c.), mice were exposed 3 times to aerosolized OVA before sacrifice. Numbers indicate days. (B) OVA-specific serum IgG1 and IgG2a at the timepoint of sacrifice were measured at a serum dilution of 1:10 000 and 1:400, respectively. Data are shown as relative light units (RLU) of a luminometric ELISA (n = 12). Background is indicated by dotted line. (C) Serum and cell-bound IgE were analyzed by RBL assay (serum dilution 1:150) and BAT, respectively. (D) Number of eosinophils in BALF and lung tissue was analyzed by flow cytometry. (E) Airway hyperresponsiveness was assessed by WBP as well as resistance and compliance (Cdyn) measurements. Penh, resistance, and compliance data are shown as area under the curve (AUC) of a methacholine challenge dose-response curve

LamOVA-induced activation of BMDCs was associated with a robust, dose-dependent cytokine and chemokine response (Figure S6). Compared to OVA and laminarin, LamOVA significantly upregulated all measured cytokines and chemokines in FL-BMDCs (two-way RM ANOVA, followed by Tukey's post hoc test). GM-BMDCs displayed a much higher basal activation status than FL-BMDCs as indicated by significantly higher levels of IL-1α, IL-1β, IFN-γ, IL-17A, IL-6, IL-27, CCL-3, CCL-4, CXCL10, CCL17, and CCL22 after 24 hours incubation without stimulus. CCL3, CCL4, CCL17, and CCL22 were especially elevated (37-, 80-, 138-, and 101-fold) compared to FL-BMDCs. Despite this higher basal activation level, LamOVA significantly upregulated pro-inflammatory mediators (TNF-α, IFN-β, IL-6, IL-23, CCL3, CCL4, CCL5, and CXCL10), and neutrophil attractants CXCL1 and CXCL5. In contrast, neither EndoFit™ OVA nor laminarin induced significant cytokine or chemokine secretion in either BMDC type.

3.5 | LamOVA activated BMDCs are potent inducers of T-cell responses

Laminarin conjugation to OVA significantly increased uptake and induced activation of BMDCs and secretion of pro-inflammatory cytokines. These properties of LamOVA conjugate also resulted in enhanced stimulation of OVA-specific naïve T cells co-cultured with BMDCs. Both, FL- and GM-BMDCs incubated with LamOVA significantly activated T-cell proliferation and cytokine secretion (Figure 3B and C). GM-BMDCs loaded with conjugates were more potent in inducing DO11.10 T-cell proliferation than FL-BMDCs, which may be due to their higher basal activation status (Figure S5). This is also supported by the fact that only GM-BMDCs could induce activation of naïve T cells (Figure 3B) and significant secretion of cytokines (IFN-γ and IL-9, Figure 3C) in the presence of Endofit™ OVA. In both cell culture models, conjugates significantly induced IL-2, IL-6, and IL-22 production ($P < .0001$, Figure 3C). Interestingly, LamOVA loaded FL- and GM-BMDCS displayed a different TH-polarizing potential as FL-BMDCs mainly generated TH1 cells (IFN-γ and TNF-α, $P < .0001$ and $P < .001$), whereas GM-BMDCs favored upregulation of IL-2, which correlated with the higher T-cell proliferation rate.

3.6 | Epicutaneous immunization with LamOVA induces a strong antibody response

We have previously shown that epicutaneous immunization with mannan-conjugated allergen via laser-generated micropores (EPI) is considerably more immunogenic compared to immunization with

unconjugated allergen.[15] In a prophylactic immunization experiment (Figure 4A), we could confirm that EPI with LamOVA induces ~threefold higher IgG1 antibody titers compared with OVA after two immunizations (Figure 4B). This immune potentiating effect was dependent on the covalent linkage between OVA and laminarin since a mix of uncoupled OVA with laminarin did not enhance antibody responses. After a second booster immunization, all groups displayed similar antibody titers (Figure 4C). IgG2a levels were close to the detection limit (data not shown).

3.7 | Preventive LamOVA immunizations reduce allergic lung inflammation and airway hyperresponsiveness

To investigate whether LamOVA-EPI would protect from allergic sensitization and lung inflammation, vaccinated mice were sensitized by two i.p. injections of Endofit™ OVA/alum followed by three aerosol challenges.

Lung function was measured by whole-body plethysmography (WBP) under methacholine challenge. Mice vaccinated with LamOVA showed the lowest Penh values, significantly lower compared to the sham-treated control group (Figure 4D). The reduction of airway hyperresponsiveness (AHR) was confirmed in selected groups by invasive resistance (R) and compliance (Cdyn) measurement on the next day, confirming the WBP results (Figure 4E and F).

After R/C measurement, the cellular composition and cytokine content of bronchoalveolar lavage fluid (BALF) were analyzed. Preventive immunizations with OVA significantly reduced the number of eosinophils (Figure 4G) in BALF, with no differences between the OVA, LamOVA, and Laminarin + OVA groups. Eosinophil counts in whole lung tissue confirmed BALF analysis for OVA and LamOVA (Figure 4H). Eotaxin and IL-5 concentration in BALF were similar in all groups and did not correlate with eosinophil number in BAL and lung tissue (data not shown).

In summary, our data show that despite their hypoallergenicity, conjugates are more potent in the production of OVA-specific IgG antibodies and can prevent allergic sensitization and airway hyperresponsiveness. In a next step, we therefore evaluated safety and potency of LamOVA conjugates in a therapeutic mouse model of allergic asthma.

3.8 | Epicutaneous immunotherapy with LamOVA induces blocking IgG and suppresses lung inflammation

In a therapeutic experiment, mice were sensitized by two i.p. injections of 10 μg Endofit™ OVA/alum followed by intranasal (i.n.) OVA challenge to induce lung inflammation. Based on WBP data, mice were stratified into five treatment groups with similar means and distribution of Penh. RBL assay confirmed that all animals had OVA-specific IgE antibodies, however, treatment arms—by

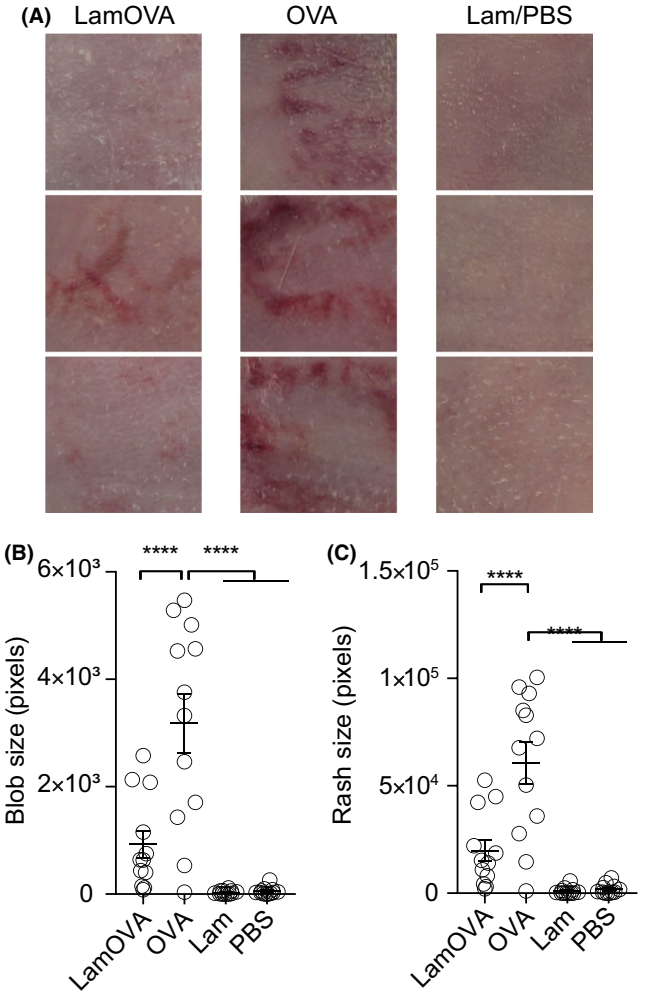

FIGURE 6 Skin erythema induced by EPIT (A) 24 hours after the 4th or 5th treatment, immunization sites were photographed and the sum of directly connected pixels of the segmented erythema (blob size, (B) and the total erythema size (C) were quantitated (n = 12). Panel A shows three representative animals from each group

chance—showed slightly higher IgE levels before therapy compared with the control groups (Figure S7). Mice were treated 8 times epicutaneously (EPIT) with either LamOVA or OVA. As a positive control, mice were treated by subcutaneous injections of Endofit™ OVA together with alum (OVA s.c.). Controls were sham treated with either PBS or laminarin (Figure 5A).

LamOVA was equally potent in inducing IgG1 antibody production compared to s.c. injections together with alum. In contrast, EPIT with unconjugated OVA elicited significantly less antibodies. Treatment with conjugates showed a trend toward increased production of IgG2a antibodies (Figure 5B).

Subcutaneous immunotherapy with OVA significantly increased serum IgE levels compared to the PBS-treated control group. The IgE increase after EPIT with LamOVA and OVA was less prominent compared to SCIT with OVA/alum (Figure 5C). It is known that AIT can temporarily increase serum IgE levels. However, more relevant is the blocking of basophil and mast cell activation induced by cross-linking

of long-lived cell-bound IgE. To test ex vivo blocking of basophil activation, blood samples were drawn 24 hours after the second exposure to aerosolized allergen and restimulated in vitro with OVA for 2 hours. Basophils from laminarin or PBS-treated control groups showed high activation levels as indicated by the strong expression of CD200R. In contrast, basophils from OVA-immunized groups showed significantly lower activation (Figure 5C). To test, whether the reduced basophil activation was due to the presence of blocking IgG, blood samples from treated mice were either washed or left untreated before in vitro restimulation with OVA. In the absence of autologous serum, basophils from all groups showed similar activation (Figure S8A), indicating the presence of comparable amounts of OVA-specific IgE on the basophils. Thus, the IgG blocking capacity can be displayed as the ratio of basophil activation in the absence or presence of autologous serum. Correlating with the ELISA data, LamOVA EPIT group and OVA s.c. group showed the highest levels of blocking IgG (Figure S8B).

EPIT groups displayed the lowest number of eosinophils in BALF and significantly lower numbers in lung tissue compared with sham-treated mice (Figure 5D). No significant differences in the BALF levels of IL-4, IL-5, IL-13, and eotaxin were found (data not shown). OVA treatment significantly improved lung function measured by WBP and again the EPIT groups showed the lowest Penh values (Figure 5E). Though not statistically significant, a trend for reduced resistance and increased compliance in the EPIT groups was confirmed by invasive R/C measurement (Figure 5E).

Restimulation of splenocytes with OVA (10 μg/mL) induced increased expression of TH2 associated cytokines IL-4, IL-5, IL-10, and IL-13 but also IFN-γ, IL-2, IL-6, and IL-22 in the s.c. OVA group and surprisingly also in the group treated with laminarin alone. EPIT groups showed no such boost in cytokine responses and remained at similar levels compared with the PBS-treated group (Figure S9). This effect was also seen on the level of transcription factor expression Tbet, GATA3, and RORγT. No difference in the number of FoxP3 + CD25+ Tregs was found in the spleens (Figure S10). In summary, s.c. injection with OVA/alum as well as treatment with laminarin boosted mainly TH2, but also TH1 and TH22 responses, whereas EPIT with OVA or LamOVA induced no increase in cytokine responses compared to the untreated group.

3.9 | Conjugation of polysaccharide to OVA reduces local side effects in vivo

In mice, local side effects are dependent on the used allergen. While in previous studies with recombinant Phl p 5[28] or depigmented house dust mite extract,[29] no local side effects were observed, application of OVA to the skin of sensitized mice led to significant skin erythema and scab formation (Figure 6A). We quantitated local skin reactions by calculating total erythema size and blob size (Figure 6B and C) and found that LamOVA immunizations induced significantly lower skin reactions, confirming the hypoallergenicity observed in vitro. The use of laser with PBS and laminarin alone did not induce any side effects, confirming the antigen-specificity of the response.

4 | DISCUSSION

Allergen-specific immunotherapy (AIT) is the only disease-modifying approach for treatment of allergies. However, classical subcutaneous immunotherapy (SCIT) suffers from low patient compliance due to exhaustive treatment protocols and occurrence of local and systemic adverse reactions. Therefore, more efficient and safe therapeutic concepts are urgently needed. Subcutaneous injections deliver antigen into the hypodermis, an adipose tissue rich in blood vessels, but sparsely populated by APCs. In contrast, epidermis and dermis are rich in APCs and (epi)cutaneous immunotherapy may result in enhanced immunogenicity and efficacy. Delivery of allergen to superficial skin layers avoids contact with blood vessels, decreasing the risk of systemic side effects.[30,31] Upon epicutaneous application, antigen is taken up by Langerhans and dendritic cells, which migrate to the lymph nodes for presentation of antigenic peptides to T cells. In a peanut allergy model, EPIT with Viaskin® occlusive patches led to formation of tolerogenic immune responses,[31] demonstrating an important role of Langerhans cells in induction of regulatory T cells (Treg) in the context of skin immunization. Other APCs, which are able to generate Tregs, such as the CD11b + cDC2 subset, have been shown to reside in the dermis.[32,33] Though epicutaneous allergen delivery with occlusive patches has been shown to effectively induce tolerance, this approach affords high amounts of allergen to be daily applied over several years[4] due to limited penetration of antigen through the outermost skin layer, the stratum corneum. In contrast, pretreatment of the skin for disruption of this tight barrier can improve immunogenicity of EPIT. This approach has been introduced in Europe during the 1950s and has only recently proven its potency to reduce allergic symptoms in clinical trials.[2] In this work, we utilized an infrared laser (PLEASE® Professional) device for controlled and highly reproducible barrier disruption. In addition to physically breaching the stratum corneum for facilitated antigen delivery directly to skin resident APCs,[16] laser microporation creates a proinflammatory cytokine and chemokine milieu, which boosts immunogenicity.[34]

Notably, Senti et al reported that allergen application onto barrier disrupted skin may result in local and systemic side effects,[2] thus highlighting the need for hypoallergenic, yet immunogenic formulations. Coupling of carbohydrates to allergens represents an elegant approach to reduce the IgE binding capacity of the resulting neoglycoconjugates, while simultaneously targeting and stimulating dendritic cells. We have reported that mannan-Bet v 1 conjugates (Bet-MN) are particularly hypoallergenic and no longer induce basophil activation in vitro.[15,35] In a similar approach, Sirvent et al demonstrated hypoallergenicity of mannan allergoids using skin prick tests in allergic patients.[36] In our current study, we found 4-5 kD laminarin conjugates to be fivefold less allergenic in vitro (Figure 2B) and to induce significantly less local side effects in sensitized mice during therapy (Figure 6). Coupling of allergens to β-glucan molecules with

a higher molecular weight could potentially further decrease allergenicity as we have previously seen a >1000-fold reduction of IgE cross-linking capacity of 30-40 kD mannan conjugates.[15] However, a careful balance of protein/carbohydrate ratio has to be maintained, as a higher polysaccharide content in conjugates potentially decreases IgG production (unpublished observation).

Due to the low immunogenicity of existing allergy vaccines, AIT requires repetitive administrations of high allergen doses. More potent and controlled APC activation may be achieved via specific targeting of surface receptors,[6] for example, C-type lectin receptors.[37] Here, we used laminarin to target Dectin-1, which is expressed on various cell types including CD11b + dermal DCs and Langerhans cells in mice.[38] We[15,35] and others[36,39] have previously reported enhanced uptake of neoglycoconjugates compared with unconjugated protein. In contrast to Sirvent et al, who observed that oxidation of mannan impaired uptake of conjugates,[36] we have shown that mild oxidation of laminarin for allergen coupling does not influence its biological activity, as confirmed by its binding to Dectin-1 (Figure 2A) and activation of BMDCs (Figures S5 and S6). We previously made similar observations for mannan[15] and other carbohydrates.[35] We employed two different in vitro models for studying antigen uptake, DC activation, and stimulation of naïve T cells, that is, Flt3L derived BMDCs and GM-CSF derived BMDCs. While FL-BMDCs more closely represent steady state naïve DCs, GM-BMDCs rather resemble monocyte-derived inflammatory DCs (and macrophages).[20,21] Both models are relevant for skin vaccine evaluation as they represent both, the early phase of the immune response, when naïve DCs first encounter an antigen, and the late phase response, when local inflammation (induced by adjuvants or laser microporation) attracts inflammatory DCs to the vaccination site. Indeed, GM-BMDCs displayed a higher basal activation status in the absence of stimuli as indicated by increased levels of CD86 and Dectin-1 expression (Figure S5) and enhanced secretion of cytokines and chemokines (Figure S6) compared to FL-BMDCs. Laminarin is a β-1,3-glucan and, depending on the mode of uptake, can have pro- or anti-inflammatory properties. For example, low molecular weight laminarins do not stimulate APCs,[25] as Dectin-1 activation occurs only after clustering of several units of the receptor.[40] Hence, receptor oligomerization requires a specific size of β-glucan complexes.[25] Here, we demonstrate that (dialyzed) 4.5 kDa laminarin does not activate BMDCs in vitro, whereas laminarin-OVA complexes are very potent in stimulating GM-BMDCs as well as FL-BMDCs. It has been shown that receptor internalization attenuates pro-inflammatory signaling, whereas large particles such as zymosan cannot be internalized and induce strong pro-inflammatory immune responses.[41] Corroborating findings from Xie et al,[39] our data indicate that LamOVA is taken up by receptor-mediated phagocytosis as indicated by downregulation of surface Dectin-1 expression (Figure S5) and transport into the endosome (Figure 3A). Yet, in contrast to data from others,[41] we clearly observed the induction of inflammatory pathways in LamOVA stimulated BMDCs. In line with the BMDC activation status, only GM-BMDCs could activate naïve OVA-specific T cells without additional stimuli (Figure 3B and C). In contrast, BMDCs pulsed with LamOVA were potent activators of naïve T-cell proliferation and cytokine secretion. As components of fungal cell walls, β-1,3-glucans are known to trigger TH1/TH17 adaptive immunity.[38,42] This could be confirmed in T cells stimulated with LamOVA loaded FL-BMDCs, which secreted high levels of IFN-γ, TNF-α, and IL-22, and low levels of IL-17 (Figure 3C). Interestingly, although GM-DCs induced stronger T-cell proliferation and IL-2 secretion, they were less potent in inducing TH1 cytokine secretion, which also correlates with their lower levels of IL-12 secretion upon LamOVA stimulation compared to FL-BMDCs (Figure S6).

We have recently demonstrated that application of allergens to laser-microporated skin can induce humoral immune responses[16,29,43] and that conjugation to mannan potentiates antibody responses.[15] As shown previously for mannan, laminarin also boosted IgG1 responses threefold after EPI and covalent linkage of the carbohydrate to OVA was essential for this effect (Figure 4B). This can be explained by the multimeric state of laminarin, that is more potent in stimulating Dectin-1 than soluble laminarin (Figures S5 and S6), the enhanced uptake due to receptor-mediated endocytosis of the complexes (Figure 3A), and a potentially slower draining to SDLNs as previously observed for Bet-mannan conjugates.[15] A similar observation was made by Xie et al after s.c. immunization; however, they also included poly I:C as an adjuvant.[39] In a prophylactic setting, EPI with OVA and LamOVA significantly suppressed induction of allergen-induced lung inflammation. Although statistically not significant, LamOVA vaccinated animals showed lower lung resistance (Figure 4E) and higher dynamic compliance (Figure 4F) compared with OVA-immunized mice. Thus, despite priming TH1/TH17 responses in vitro, LamOVA had no detrimental inflammatory effects in a prophylactic allergy model in vivo.

We have previously shown in a therapeutic mouse model of allergic lung inflammation that laser-mediated EPIT with Phl p 5 or house dust mite extract can successfully reduce lung inflammation and improve lung function. Therapeutic efficacy was associated with induction of high levels of blocking IgG and a general downregulation of cytokine responses.[28,29] In the current study, we show for the first time the therapeutic efficacy of a hypoallergenic laminarin-allergen conjugate. While EPIT with OVA was similarly effective in suppressing allergic lung inflammation and airway hyperresponsiveness compared with LamOVA, it was associated with severe local side effects (Figure 6), replicating findings from clinical trials with grass pollen extract.[2] In contrast, LamOVA treated mice showed significantly ameliorated skin erythema. At the same time, conjugation to laminarin significantly boosted IgG1 (compared to OVA EPIT) to the same levels as achieved by s.c. injections together with alum (Figure 5A), while inducing lower levels of therapy-associated IgE (Figure 5C). Furthermore, both EPIT groups showed lower levels of lung inflammation compared to s.c. treated mice (Figure 5D and E). Although LamOVA-induced inflammation and TH1/TH17 polarization in vitro, EPIT with LamOVA did not result in enhanced inflammatory cytokine secretion in splenocytes from treated animals (Figure S9). In contrast, SCIT with

OVA boosted TH2 responses, an early therapy effect that is well known in the clinics.[44] Though we did not find increased numbers of FoxP3 + CD25+ regulatory T cells in the spleen after treatment, EPIT significantly reduced the number of activated T cells compared with SCIT (Figure S10). Taken together, this confirms our previous findings that EPIT via laser-generated micropores can downregulate established allergic responses and mainly results in the induction of blocking IgG and a general suppression of cytokines[28,29] rather than immune deviation toward TH1 or TH17, even in the presence of an immunostimulatory Dectin-1 agonist. While the first clinical studies of SCIT with mannan allergoids are currently under way (NCT02654223, NCT02661854), we believe that combining a C-type lectin receptor-based DC targeting approach with a method to deliver a hypoallergenic vaccine to upper skin layers rich in APCs is the key to patient friendly, safe and effective immunotherapy. Our current proof of concept study demonstrates that laser-facilitated EPIT with β-glucan-allergen conjugates represents one such feasible approach.

ACKNOWLEDGMENT

This work was supported by the Austrian Science Fund (FWF; grant no. W 1213).

CONFLICTS OF INTEREST

The authors declare that they have no conflict of interest.

AUTHOR CONTRIBUTIONS

EK, S. Scheiblhofer, IJ, HS, and RW performed in vivo mouse experiments. VS did in vitro BMDC experiments. M. Schubert performed NMR measurements and analysis. ED performed MST measurements and analyzed the data.TN, MS, and RB performed lung perfusions and prepared total lung digests. MG analyzed conjugates by DLS. S. Wildner and GG determined conjugate concentration by amino acid analysis. DJ, S. Schaller, and S. Winkler generated computational model and wrote the software for skin erythema analysis. RW, S. Scheiblhofer, and EK designed the study and wrote the manuscript. RW, EK, and JHH analyzed the data. S. Wildner, GG, and JHH critically revised the manuscript.

ORCID

Mario Schubert https://orcid.org/0000-0003-0278-4091
Gabriele Gadermaier https://orcid.org/0000-0002-4886-417X
Richard Weiss https://orcid.org/0000-0003-3185-7253

REFERENCES

1. Senti G, von Moos S, Kundig TM. Epicutaneous allergen administration: is this the future of allergen-specific immunotherapy? *Allergy* 2011;66(6):798-809.
2. Senti G, von Moos S, Tay F, Graf N, Johansen P, Kundig TM. Determinants of efficacy and safety in epicutaneous allergen immunotherapy: summary of three clinical trials. *Allergy* 2015;70(6):707-710.
3. Dupont C, Kalach N, Soulaines P, Legoue-Morillon S, Piloquet H, Benhamou PH. Cow's milk epicutaneous immunotherapy in children: a pilot trial of safety, acceptability, and impact on allergic reactivity. *J Allergy Clin Immunol.* 2010;125(5):1165-1167.
4. Jones SM, Sicherer SH, Burks AW, et al. Epicutaneous immunotherapy for the treatment of peanut allergy in children and young adults. *J Allergy Clin Immunol.* 2017;139(4):1242-1252.e9.
5. Hung IFN, Yuen KY. Immunogenicity, safety and tolerability of intradermal influenza vaccines. *Hum Vaccin Immunother.* 2018;14(3):565-570.
6. Fehres CM, Garcia-Vallejo JJ, Unger WW, van Kooyk Y. Skin-resident antigen-presenting cells: instruction manual for vaccine development. *Front Immunol.* 2013;4:157.
7. Geijtenbeek TB, Gringhuis SI. C-type lectin receptors in the control of T helper cell differentiation. *Nat Rev Immunol.* 2016;16(7):433-448.
8. Willment JA, Marshall AS, Reid DM, et al. The human beta-glucan receptor is widely expressed and functionally equivalent to murine Dectin-1 on primary cells. *Eur J Immunol.* 2005;35(5):1539-1547.
9. Gour N, Lajoie S, Smole U, et al. Dysregulated invertebrate tropomyosin-dectin-1 interaction confers susceptibility to allergic diseases. *Sci Immunol.* 2018;3(20):eaam9841.
10. Reid DM, Montoya M, Taylor PR, et al. Expression of the beta-glucan receptor, Dectin-1, on murine leukocytes in situ correlates with its function in pathogen recognition and reveals potential roles in leukocyte interactions. *J Leukoc Biol.* 2004;76(1):86-94.
11. Cohen-Kedar S, Baram L, Elad H, Brazowski E, Guzner-Gur H, Dotan I. Human intestinal epithelial cells respond to beta-glucans via Dectin-1 and Syk. *Eur J Immunol.* 2014;44(12):3729-3740.
12. Heyl KA, Klassert TE, Heinrich A, et al. Dectin-1 is expressed in human lung and mediates the proinflammatory immune response to nontypeable Haemophilus influenzae. *MBio.* 2014;5(5):e01492-e11414.
13. Kobayashi M, Yoshiki R, Sakabe J, Kabashima K, Nakamura M, Tokura Y. Expression of toll-like receptor 2, NOD2 and dectin-1 and stimulatory effects of their ligands and histamine in normal human keratinocytes. *Br J Dermatol.* 2009;160(2):297-304.
14. Song K, Xu LI, Zhang W, et al. Laminarin promotes anti-cancer immunity by the maturation of dendritic cells. *Oncotarget.* 2017;8(24):38554-38567.
15. Machado Y, Duinkerken S, Hoepflinger V, et al. Synergistic effects of dendritic cell targeting and laser-microporation on enhancing epicutaneous skin vaccination efficacy. *J Control Release.* 2017;266:87-99.
16. Weiss R, Hessenberger M, Kitzmüller S, et al. Transcutaneous vaccination via laser microporation. *J Controlled Release* 2012;162(2):391-399.
17. Wang J, Shah D, Chen X, Anderson RR, Wu MX. A micro-sterile inflammation array as an adjuvant for influenza vaccines. *Nat Commun.* 2014;5:4447.
18. Laurentin A, Edwards CA. A microtiter modification of the anthrone-sulfuric acid colorimetric assay for glucose-based carbohydrates. *Anal Biochem.* 2003;315(1):143-145.
19. Wildner S, Elsässer B, Stemeseder T, et al. Endolysosomal degradation of allergenic ole e 1-like proteins: analysis of proteolytic cleavage sites revealing T cell epitope-containing peptides. *Int J Mol Sci.* 2017;18(8):1780.
20. Helft J, Böttcher J, Chakravarty P, et al. GM-CSF mouse bone marrow cultures comprise a heterogeneous population of CD11c(+)MHCII(+) macrophages and dendritic cells. *Immunity* 2015;42(6):1197-1211.
21. Xu Y, Zhan Y, Lew AM, Naik SH, Kershaw MH. Differential development of murine dendritic cells by GM-CSF versus Flt3 ligand has implications for inflammation and trafficking. *J Immunol.* 2007;179(11):7577-7584.
22. Teodorowicz M, Perdijk O, Verhoek I, et al. Optimized Triton X-114 assisted lipopolysaccharide (LPS) removal method

reveals the immunomodulatory effect of food proteins. *PLoS One* 2017;12(3):e0173778.
23. Petersen BO, Krah M, Duus JO, Thomsen KK. A transglycosylating 1,3(4)-beta-glucanase from rhodothermus marinus NMR analysis of enzyme reactions. *Eur J Biochem*. 2000;267(2):361-369.
24. Read SM, Currie G, Bacic A. Analysis of the structural heterogeneity of laminarin by electrospray-ionisation-mass spectrometry. *Carbohydr Res*. 1996;281(2):187-201.
25. Smith AJ, Graves B, Child R, et al. Immunoregulatory activity of the natural product laminarin varies widely as a result of its physical properties. *J Immunol*. 2018;200(2):788-799.
26. Willard L, Ranjan A, Zhang H, et al. VADAR: a web server for quantitative evaluation of protein structure quality. *Nucleic Acids Res*. 2003;31(13):3316-3319.
27. Willment JA, Lin H-H, Reid DM, et al. Dectin-1 expression and function are enhanced on alternatively activated and GM-CSF-treated macrophages and are negatively regulated by IL-10, dexamethasone, and lipopolysaccharide. *J Immunol*. 2003;171(9):4569-4573.
28. Bach D, Weiss R, Hessenberger M, et al. Transcutaneous immunotherapy via laser-generated micropores efficiently alleviates allergic asthma in Phl p 5–sensitized mice. *Allergy* 2012;67(11):1365-1374.
29. Korotchenko E, Moya R, Scheiblhofer S, et al. Laser facilitated epicutaneous immunotherapy with depigmented house dust mite extract alleviates allergic responses in a mouse model of allergic lung inflammation. *Allergy*. 2020;75(5):1217-1228.
30. Dioszeghy V, Mondoulet L, Dhelft V, et al. Epicutaneous immunotherapy results in rapid allergen uptake by dendritic cells through intact skin and downregulates the allergen-specific response in sensitized mice. *J Immunol*. 2011;186(10):5629-5637.
31. Mondoulet L, Dioszeghy V, Thebault C, Benhamou PH, Dupont C. Epicutaneous immunotherapy for food allergy as a novel pathway for oral tolerance induction. *Immunotherapy*. 2015;7(12):1293-1305.
32. Dioszeghy V, Mondoulet L, Laoubi L, et al. Antigen uptake by langerhans cells is required for the induction of regulatory T cells and the acquisition of tolerance during epicutaneous immunotherapy in OVA-sensitized mice. *Front Immunol*. 2018;9:1951.
33. Tordesillas L, Lozano-Ojalvo D, Dunkin D, et al. PDL2(+) CD11b(+) dermal dendritic cells capture topical antigen through hair follicles to prime LAP(+) Tregs. *Nat Commun*. 2018;9(1):5238.
34. Kashiwagi S, Brauns T, Poznansky MC. Classification of laser vaccine adjuvants. *J Vaccines Vaccin*. 2016;7(1):307.
35. Weinberger EE, Himly M, Myschik J, et al. Generation of hypoallergenic neoglycoconjugates for dendritic cell targeted vaccination: a novel tool for specific immunotherapy. *J Controlled Release* 2013;165(2):101-109.
36. Sirvent S, Soria I, Cirauqui C, et al. Novel vaccines targeting dendritic cells by coupling allergoids to nonoxidized mannan enhance allergen uptake and induce functional regulatory T cells through programmed death ligand 1. *J Allergy Clin Immunol*. 2016;138(2):558-567.e511.
37. Weiss R, Scheiblhofer S, Machado Y, Thalhamer J. New approaches to transcutaneous immunotherapy: targeting dendritic cells with novel allergen conjugates. *Curr Opin Allergy Clin Immunol*. 2013;13(6):669-676.
38. Kashem SW, Igyártó BZ, Gerami-Nejad M, et al. Candida albicans morphology and dendritic cell subsets determine T helper cell differentiation. *Immunity* 2015;42(2):356-366.
39. Xie J, Guo L, Ruan Y, et al. Laminarin-mediated targeting to Dectin-1 enhances antigen-specific immune responses. *Biochem Biophys Res Comm* 2010;391(1):958-962.
40. Goodridge HS, Underhill DM, Touret N. Mechanisms of Fc receptor and dectin-1 activation for phagocytosis. *Traffic* 2012;13(8):1062-1071.
41. Hernanz-Falcón P, Joffre O, Williams DL, Reis e Sousa C. Internalization of Dectin-1 terminates induction of inflammatory responses. *Eur J Immunol*. 2009;39(2):507-513.
42. Carvalho A, Giovannini G, De Luca A, et al. Dectin-1 isoforms contribute to distinct Th1/Th17 cell activation in mucosal candidiasis. *Cell Mol Immunol*. 2012;9(3):276-286.
43. Hessenberger M, Weiss R, Weinberger EE, Boehler C, Thalhamer J, Scheiblhofer S. Transcutaneous delivery of CpG-adjuvanted allergen via laser-generated micropores. *Vaccine* 2013;31(34):3427-3434.
44. Akdis M, Akdis CA. Mechanisms of allergen-specific immunotherapy. *J Allergy Clin Immunol*. 2007;119(4):780-791.

SUPPORTING INFORMATION

Additional supporting information may be found online in the Supporting Information section.

How to cite this article: Korotchenko E, Schießl V, Scheiblhofer S, et al. Laser-facilitated epicutaneous immunotherapy with hypoallergenic beta-glucan neoglycoconjugates suppresses lung inflammation and avoids local side effects in a mouse model of allergic asthma. *Allergy*. 2020;00:1–13. https://doi.org/10.1111/all.14481

Supporting Information

Laser-facilitated epicutaneous immunotherapy with hypoallergenic beta-glucan neoglycoconjugates suppresses lung inflammation and avoids local side effects in a mouse model of allergic asthma

Evgeniia Korotchenko [a], Viktoria Schießl [a], Sandra Scheiblhofer [a], Mario Schubert [a], Elfriede Dall [a], Isabella Joubert [a], Helen Strandt [a], Theresa Neuper [a], Muamera Sarajlic [a], Renate Bauer [a], Mark Geppert [a], David Joedicke [b], Sabrina Wildner [a], Susanne Schaller [b], Stephan Winkler [b], Gabriele Gadermaier [a], Jutta Horejs-Hoeck [a], Richard Weiss [a*]

[a] University of Salzburg, Department of Biosciences, Salzburg, Austria

[b] University of Applied Biosciences Upper Austria, Research and Development, Hagenberg, Austria

[*] to whom correspondence should be addressed: Richard.Weiss@sbg.ac.at

Supplementary Methods

NMR spectroscopy

All NMR data were measured on a 600 MHz Avance III HD spectrometer (Bruker Biospin) equipped with a $^{1}H/^{13}C/^{15}N/^{31}P$ QXI probe at 298 K. The lyophilized samples were dissolved in D_2O (100%D, Armar, Germany) and measured in 5 mm tubes. Spectra were referenced to 2,2-dimethyl-2-silapentanesulfonic acid (DSS) using an external sample of 2 mM sucrose 0.5 mM DSS in H_2O/D_2O (Bruker Biospin). The ^{13}C axis was indirectly referenced using the recommended scaling factor Ξ of 0.251449530 according to IUPAB [1]. Standard 2D ^{1}H-^{13}C HSQC spectra were recorded with 2018 and 13.9 ppm spectral width for ^{1}H and 250 data points and 82.8 ppm spectral width using 64 scans, a recycle delay of 4 sec resulting in a measurement time of ~19 hours. 2D ^{1}H-^{1}H TOCSY spectra were collected with 2018 and 11.7 ppm spectral width for ^{1}H and 512 data points and 10.4 ppm spectral width using 4 scans, mixing times of 80 ms or 12 ms, a recycle delay of 1 sec resulting in a measurement time of approx. 50 min. 2D ^{1}H-^{1}H NOESY spectra were acquired with 2018 data points and 10.0 ppm spectral width for ^{1}H and 700 data points and 10.0 ppm spectral width using 40 scans, a mixing time of 120 ms, a recycle delay of 1 sec resulting in a measurement time of 11 hours. 2D ^{1}H-^{13}C HMBC spectra were measured using the pulse sequence hmbclpndqf (Bruker Biospin) with 4096 points and 20 ppm spectral width for ^{1}H and 512 data points and 222 ppm spectral width for ^{13}C, 64 scans, optimized for a J_{CH} long range coupling of 8 Hz, a recycle delay of 1.5 sec resulting in a measurement time of 17 hours. 2D ^{1}H-^{13}C HSQC-TOCSY spectra were recorded using the pulse sequence hsqcdietgpsisp.2 (Bruker Biospin) with 1024 and 16 ppm spectral width for ^{1}H and 512 data points and 49.5 ppm spectral width, using 128 scans, a recycle delay of 1.2 sec and mixing times of 12 ms or 82 ms, resulting in a measurement time of ~24 hours Data were processed with Topspin 3.2 (Bruker Biospin, Germany) and the chemical shift assignment was achieved using the software Sparky 3.115 (T. D. Goddard and D. G. Kneller, SPARKY 3, University of California, San Francisco).

Laminarin binding assays

Binding of soluble murine dectin-1a receptor (fused to an IgG1 Fc domain, Invivogen) to plate-bound OVA or LamOVA was assessed by ELISA. Briefly, a 96-well F-bottom plate was coated overnight with 10 µg/mL OVA or LamOVA in PBS. The next day, unbound molecules were removed by washing with PBS, 0.02% Tween followed by blocking with a polymer based blocking reagent (ROTI™Block, Carl Roth) for 1h at room temperature. Subsequently, increasing concentrations of Fc-dectin-1a (Dec-1a) were added starting from 2 ng/mL. The highest concentration was 2 µg/mL. After incubation for 1h

at RT the plate was washed, and HRP-conjugated anti-human IgG1 (Biolegend) was added (dilution 1:500) and incubated for 1h at RT. After washing, the assay was developed by addition a of Chemiluminescence ELISA substrate (Roche).

Interaction of OVA, LamOVA or laminarin with Fc-dectin-1a in solution was measured by Microscale Thermphoresis (MST) using a Monolith NT.115 RED instrument (Nanotemper, Munich, Germany). 50 µg of Dec-1a or soluble human TLR5 fused to an IgG1 Fc domain (TLR5, used as unspecific binding control), were buffer exchanged into 1x PBS buffer. Subsequently, the receptors were covalently labeled with NT-647-NHS dye (Nanotemper) at a molar ratio of 1:3 (protein:dye) in PBS buffer for 30 min at 20 °C in the dark. Unreacted, excess dye was removed using a NAP-5 column (GE Healthcare) preequilibrated in PBS buffer and DOL (degree of labeling) and protein concentration were determined according to the manufacturer's instructions. To determine the binding affinity of LamOVA, OVA, and 4.5kD laminarin, a 1:2 dilution series was prepared in PBST buffer (PBS + 0.05% Tween-20). Based on the assumption that 1 OVA molecule (45 kDa) was modified on average with 6 laminarin moieties (4.5 kDa each), the concentration of the LamOVA stock solution was 2.2 mg/ml (51 µM) based on OVA and 1.3 mg/ml (288 µM) based on laminarin. Labeled Dec-1a or TLR5 were diluted 1:50 in PBST buffer, to reach a final concentration of 4.4 nM. 10 µl of the respective sample dilution were mixed with 10 µl of the labeled receptors and incubated for 15 min at 20 °C in the dark. To remove possible aggregates, the complexes were centrifuged at 13.000 g for 15 min at 4°C. Immediately after centrifugation, the reactions were transferred into standard coated capillaries and MST traces were measured at 25 °C, 50% LED and medium MST power in an NT.115 RED instrument. Data were recorded with the MO.Control 1.5.1 (NanoTemper) software and further analyzed using MO-Affinity Analysis 2.2.6 (NanoTemper). MST traces were processed using an MST on-time of 2.5 sec and fitted using Hill (assuming multiple binding sites) fit model. EC50 values were determined from three independent binding experiments. To confirm that the shift in MST signal was due to complex formation rather than unspecific aggregation, samples were incubated with 10% SDS and 10 mM DTT and heated to 95 °C for 5min before measuring MST traces.

Generation of bone marrow-derived dendritic cells

Bone marrow was harvested from femur and tibia of BALB/c mice. For generation of FL-BMDCs, 3 mL of a $2.5x10^6$ cells/mL bone marrow cell suspension were seeded into non-cell culture treated 6-well plates and stimulated with 200ng/mL human Flt3-L for 9 days at 37°C, 5% CO_2 and 95% humidity. Between days 4 and 6, 1.5 mL of culture medium (RPMI/1640 supplemented with 2.5 mM HEPES, 100 IU/mL penicillin, 100 mg/mL streptomycin, 2 mM L-glutamine, 10% fetal calf serum) were added to each well. For generation of GM-BMDCs, 10 mL of a $2x10^5$ cells/mL bone marrow cell suspension

were plated into non-cell culture treated petri dishes and incubated in the presence of murine GM-CSF for 8 days. On day 3, 10 mL of GM-CSF containing culture medium (RPMI/1640 supplemented with 20 ng/mL GM-CSF, 100 IU/mL penicillin, 100 mg/mL streptomycin, 2 mM L/Glutamine, 10% FCS and 50 µM 2-mercaptoethanol) was added to each well, and on day 5, 10 mL medium was replaced.

Conjugate uptake, BMDC activation and T cell proliferation

To assess uptake of glycoconjugates by BMDCs, their activation, and their capacity to induce T cell proliferation, FL-BMDCs and GM-BMDCs harvested on days 9 and 8, respectively were used.

For uptake analysis, OVA and LamOVA were labeled with Invitrogen pHrodo™ iFL Green STP Ester (ThermoFisher Scientific) according to the manufacturer's protocol. Briefly, pHrodo was resuspended in DMSO to a concentration of 10 mM. For labeling, 50 µL OVA or glycoconjugates were mixed with 5 µL of a 1M $NaHCO_3$ solution (pH 8.3), added to the dye and incubated at RT for 60 min in the dark. The coupling reaction was stopped by addition of 1/10 volume of 1 M Tris pH8 followed by another incubation for 60 min at RT in the dark. Unreacted dye was removed from the samples by running over an Illustra NAP-5 column (GE healthcare). Labeled OVA and conjugates were analyzed for their fluorescence intensity at an excitation wavelength of 488nm and an emission wavelength scan between 520 and 560nm. Exact protein concentrations were determined by amino-acid analysis.

$1.5x10^5$ cells were stimulated overnight at 37°C, 5% CO_2, 95% humidity with 5µg of labeled conjugates or OVA, respectively. Incubation with PBS served as negative control. To analyze CD86 and Dectin-1 expression, $1.5x10^5$ cells were stimulated with 5, 25 or 50 µg/mL OVA or an equivalent amount of LamOVA, 12.5, 62.5 or 125 µg/mL laminarin, 1µg/mL LPS (positive control), or PBS (negative control), respectively, overnight at 37°C, 5% CO_2, 95% humidity. Cells were analyzed by flow cytometry on a Cytoflex S flow cytometer (Beckman Coulter). See suppl. Fig. 11 for gating strategy.

For T cell – BMDC co-cultures, OVA-specific T cells harvested from BALB/c DO11.10 mice were labeled with 1 µM fluorescent dye carboxyfluorescein diacetate succinimidyl ester (CFSE) in PBS. Briefly, lymph node and spleen cell suspensions were incubated for 10 minutes at 37°C in a water bath with CFSE. The reaction was stopped by addition of 10% FCS. After washing, the cells were resuspended in T cell medium (RPMI-1640 supplemented with 25 mM HEPES, 100 IU/mL penicillin, 100 mg/mL streptomycin, 2 mM L-glutamine, 10% FCS) and stained with anti-CD62L – APC-eFluor780 and anti-CD4 – eFluor450 for sorting of naïve T cells on a BD FACS Aria™ III cell sorter (BD Biosciences). Naïve DO11.10 T cells ($1x10^5$ cells/mL) and BMDCs ($0.33x10^5$ cells/mL) were co-cultured in T cell medium in the presence of 50 µg/mL OVA or an equivalent amount of conjugates or medium

for 5 days at 37°C, 5% CO_2, 95% humidity. To determine the percentage of proliferating cells, staining with anti-CD4-PerCP-Cy5.5 and fixable viability dye APC-eFluor 780 was performed and cells were analyzed by flow cytometry. Culture supernatants were used for cytokine secretion analysis by LEGENDPlex assay according to manufacturer's protocol.

BAL

Bronchoalveolar lavages were performed as described previously [2]. Following staining with anti-CD8-FITC, anti-SiglecF-PE, anti-CD45-PerCp-Cy5.5, anti-CD4-BV421, anti-CD19-PE/Cy7, and anti-Ly6G/Ly6C (Gr1)-APC, cells were analyzed by flow cytometry. Leucocytes were gated on a SSC vs. CD45 plot followed by doublets exclusion. Neutrophils were determined as $Gr1^{high}$ Siglec F^{low}, and $Gr1^{low}$ Siglec F^{high} cells were further divided into eosinophils and alveolar macrophages based on autofluorescence in the BV510 channel. $Gr1^{neg}$ Siglec F^{neg} lymphocytes were further separated into CD4 and CD8 T cells. See suppl. Fig. 12 for gating strategy.

Lung digestion

After transcardial perfusion, the right lung lobe was cut into 1x1mm pieces in digestion buffer containing Liberase™ (0.25 mg/mL, Roche), Hyaluronidase (1 mg/mL, Sigma), DNAse I (0.03 mg/mL, Sigma) and Collagenase XI (0.25 mg/mL, Sigma) in RPMI-1640 and incubated on a rotary shaker (300rpm, 30min, 37°C). Thereafter, the cell suspension without visible clumps was placed on ice and the remaining tissue was passed through a 21G needle and combined with 2 mL of fresh digestion buffer. The suspension was incubated for additional 30 min under the same conditions. The cells were pooled and EDTA was added to a final concentration of 10mM. The sample was filtered through a 100µm cell strainer (Greiner Bio One) and labeled (15min, 4°C) with biotin anti-mouse CD45.2 antibody diluted 1:50 in FACS buffer (PBS, 1% BSA, 2mM EDTA) and sorted using BD IMag™ Streptavidin Particles Plus – DM (BD Biosciences). Prior to staining, non-specific binding sites were blocked by resuspending cells in 20µL hybridoma supernatant containing anti-CD16/CD32 for 5 min at 4°C. Finally, the cell pellet was stained using the following anti-mouse antibodies: CD11b-PerCp/Cy5.5, CD45-eFluor506, GR-1-AlexaFluor700, Siglec F-Superbright 600, CD24-PE/Dazzle 594, MHC II-FITC. After incubation for 30 min at 4°C, cells were washed tree times. Finally, the pellet was resuspended in FACS buffer and cells were analyzed on a Cytoflex S flow cytometer (Beckman Coulter). Samples were analyzed according to the gating strategy published by Misharin et al. [3] (Suppl. Fig. 13).

Basophil activation test (BAT)

Cell-bound IgE was analyzed *ex vivo* by basophil activation test [4]. Whole blood was drawn from vena saphena the day after the second aerosol challenge. To prevent coagulation, 10% v/v Li-Heparin (10mg/mL in DPBS) was added. 30µL of heparinized blood was either used untouched or washed three times with 200µL of RPMI (260g, RT, 5min) to remove serum containing blocking IgGs. 30µL of RPMI with or without 2ng/mL OVA was added to the samples and incubated for 2h at 37°C, 5% CO2, 95% humidity. Subsequently, samples were put on ice and all further steps were performed with ice-cold solutions at 4°C. Samples were washed with 120µL FACS buffer and pelleted (5min centrifugation at 260 g). Cells were stained in 30µL of FACS buffer containing anti-mouse IgE-FITC, anti-CD4-PerCp-Cy5.5, anti-CD19-PE/Cy7, and anti-CD200R-APC for 20 min on ice, washed with 200µL FACS buffer, and the pellets were resuspended in red blood cell lysis buffer (eBioscience) and incubated for 5min at RT followed by two washing steps with FACS buffer. Finally, cells were resuspended in 50µL FACS buffer and analyzed by flow cytometry on a FACS Canto II flow cytometer (BD Biosciences). Basophils were gated as IgE^{high} $CD19^{neg}$ $CD4^{neg}$ and the basophil activation status was assessed as median fluorescence intensity of CD200R.

Flow Cytometry of restimulated splenocytes

Cell pellets from restimulated cells were centrifuged for 5min at 400g at 4°C. After one wash with 150µL DPBS, pellets were resuspended in 20 µL hybridoma supernatant containing anti-CD16/32 to block Fc-receptors. After 5min incubation at 4°C, 20 µL of extracellular staining mix was added directly to the samples. Extracellular staining mix contained fixable viability dye eFluor 506, anti-CD44-BV650, anti-CD25-Super Bright 600 anti-CD4-APC-eFluor780 diluted in DPBS. Plates were briefly mixed on an oscillating shaker and incubated for 30 min at 4°C in the dark. Subsequently, 100µL of ice-cold FACS buffer were added, and cells were pelleted (400g, 4 min, 4°C). Cell pellets were resuspended in 150 µL ice-cold Fix/Perm buffer (Foxp3/Transcription Factor Staining Buffer Kit, Tonbo Biosciences) and incubated 60min at 4°C in the dark. After centrifugation (400g, 4min, 4°C), pellets were washed twice in 100 µL Perm buffer from the same kit. Pellets were resuspended in 30 µL of Perm buffer containing anti-FoxP3-APC and GATA3-BV421. Samples were incubated for 30 min at RT in the dark. After one more wash with 100 µL Perm buffer, cell pellets were resuspended in 80 µL FACS buffer and analyzed on a Cytoflex S flow cytometer (Beckman Coulter). See suppl. Fig. 14 for gating strategy.

Supplementary Tables

Supplementary Table 1. Antibodies used in the study.

Marker	Fluorophore	Final Dilution	Clone	Manufacturer
BMDC stimulation, BMDC-DO11 T cell co-culture				
CD11b	PerCP-Cy5.5	1:500	M1/70	BioLegend
CD11c	BV421	1:100	N418	BioLegend
CD86	BV605	1:200	GL-1	BioLegend
Dectin-1	PE	1:100	RH1	BioLegend
Fixable viability dye	APC-eFluor780	1:3000		Invitrogen
Lung digestion				
CD11b	PerCp-Cy5.5	1:200	M1/70	BioLegend
CD24	PE/Dazzle 594	1:600	M1/69	Biolegend
CD45	eFluor 506	1:100	30-F11	Invitrogen
GR-1	Alexa Fluor 700	1:200	RB6-8C5	Biolegend
MHC II	FITC	1:200	M5/114.15.2	BioLegend
Siglec F	Superbright 600	1:200	1RNM44N	Invitrogen
BAL				
CD4	BV421	1:200	RM4-5	Invitrogen
CD45	PerCP-Cy5.5	1:400	A20	Invitrogen
GR-1	APC	1:200	RB6-8C5	Invitrogen
Siglec F	PE	1:200	E50-2440	BD
CD8	FITC	1:100	53-6.7	Invitrogen
CD19	PE-Cy7	1:100	1D3	Invitrogen
Lymphocyte restimulation				
CD4	APC-eFluor780	1:400	RM4-5	Invitrogen
CD25	Superbright 600	1:100	PC61.5	Invitrogen
CD44	BV650	1:50	IM7	Biolegend
FoxP3	APC	1:100	FJK-16s	Invitrogen
GATA3	BV421	1:100	16E10A23	BioLegend
Fixable viability dye	eFluor 506	1:1000		Invitrogen
BAT				
CD4	PerCp-Cy5.5	1:200	GK1.5	BioLegend
CD19	PE-Cy7	1:200	eBio1D3 (1D3)	eBioscience
IgE	FITC	1:200	RME-1	BioLegend
CD200R	APC	1:200	OX110	Invitrogen

Supplementary Table 2: Observed chemical shifts of dialysed laminarin dissolved in D_2O measured at 298 K in comparison to previously reported data (Petersen et al. 2000, Eur. J. Biochem 267, 361)

Moiety		H1	H1'	H2	H3	H4	H5	H6	H6'	C1	C2	C3	C4	C5	C6	
M	Mannitol	4.195	3.847	3.910	3.891	3.801	3.769	3.873	3.681	74.6	72.4	71.7	71.9	73.5	66.0	this work
		4.168	3.850	3.910	3.865	3.820	3.765	3.854	3.684	74.5	72.5	72.8[a]	72.0	71.9[a]	65.9	Petersen et al.[b]
a	3Glc3	4.801	–	3.574	3.793	3.523	3.528	3.932	3.749	105.3	76.0	86.9	70.8	78.4	63.4	this work
		4.780	–	3.573	3.786	3.537	3.515	3.928	3.747	105.4	75.9	87.0	70.8	78.3	63.4	Petersen et al.[b]
b	3Glc1M	4.548	–	3.544	3.775	n.d.[c]	3.518	3.938	n.d.[c]	105.4	75.8	86.9	70.9	78.3	n.d.[c]	this work
		4.544	–	3.544	3.768	3.510	3.510	3.928	3.750	105.4	75.6	87.1	70.9	78.3	63.4	Petersen et al.[b]
c (α)	3Glcα	5.242	–	3.735	3.924	3.530	3.871	n.d.[c]	n.d.[c]	94.8	73.8	85.0	n.d.[c]	74.0	n.d.[c]	this work
		5.242	–	3.727	3.921	3.522	3.886	3.845	3.779	94.8	73.5	85.2	n.d.[c]	n.d.[c]	n.d.[c]	Petersen et al.[b]
c (β)	3Glcβ	4.685	–	3.446	3.754	3.509	n.d.[c]	3.903	n.d.[c]	98.4	76.6	87.2	70.9	78.3	n.d.[c]	this work
		4.673	–	3.440	3.735	3.530	3.898	3.898	3.750	98.4	n.d.[c]	n.d.[c]	n.d.[c]	n.d.[c]	n.d.[c]	Petersen et al.[b]
d	Glc3Glc3	4.759	–	3.374	3.529	3.418	3.497	3.926	3.737	105.6	76.2	78.3	72.3	78.3	63.5	this work
		4.740	–	3.380	3.535	3.426	3.491	3.919	3.730	105.6	76.1	78.3	72.3	78.3	63.4	Petersen et al.[b]
e	3(6)Glc3	4.775	–	3.590	3.804	3.604[d]	3.703[d]	4.235	3.898	105.3	76.0	86.7	70.9	77.3	71.6	this work
		4.759	–	3.586	3.795	3.594	3.698	4.209	3.886	105.4	75.8	86.9	70.9	77.2	71.5	Petersen et al.[b]
f	Glc6	4.540	–	3.319	3.500	3.411	3.464	3.919	3.747	105.5	75.9	78.3	72.3	78.6	63.5	this work
		4.520	–	3.319	3.505	3.405	3.455	3.911	3.733	105.6	75.9	78.4	72.3	78.4	63.4	Petersen et al.[b]
g	3Glc6(3)Glc3	4.567	–	3.513	3.745	n.d.[c]	n.d.[c]	3.925	n.d.[c]	105.3	75.7	87.2	70.9	78.3	n.d.[c]	this work
		4.560	–	3.519	3.725	3.490	3.510	3.921	3.729	105.4	75.9	87.3	70.9	78.3	63.4	Petersen et al.[b]
h	Glc3Glc6	4.731	–	3.374	3.532	n.d.[c]	n.d.[c]	3.916	3.727	105.6	76.2	78.3	72.3	78.8	n.d.[c]	this work
		4.709	–	3.378	3.482	3.430	3.533	3.819	3.730	105.7	76.1	78.3	72.3	78.3	63.2	Petersen et al.[b]
i	6Glc3	4.732	–	3.382	3.536	3.486	3.666	4.231	3.877	105.3	76.2	78.3	72.2	77.5	71.5	this work
		4.714	–	3.391	3.540	3.480	3.672	4.203	3.872	105.7	76.0	78.3	70.9	77.5	71.5	Petersen et al.[b]
j	unknown [e]	4.855	–	3.589	3.652	3.521	3.416	3.958	3.755	105.9	n.d.[c]	88.9	70.3	79.6	n.d.[c]	this work

[a] reported values are likely incorrect, chemical shifts of mannitol form the Madison Metabolomics Consortium (entry bmse000099; doi:10.13018/BMSE000099) report 71.9, 71.9, 73.49 and 65.92 ppm for C3, C4, C5 and C6, respectively.

[b] reported chemical shifts of laminarin from *Laminaria digitata* (Sigma), 1.2 ppm were added to the reported ^{13}C chemical shifts to achieved a comparable referencing to DSS

[c] n.d. stands for not determined, mainly due to overlapping chemical shift correlations

[d] resonances are broadened, likely due to the locally increased tumbling time due to branching or local dynamics

[e] spin system not reported by Petersen et al, the ^{13}C chemical shift of C3 indicates a substitution at O3, the chemical shifts of H6 and H6' point to the lack of substitution at O6, suggesting a backbone moiety with β1,3 linkages on both sides, all signals show line broadening hinting that this moiety is close to a branch side, e.g. 3**Glc**3(6)Glc3 or 3(6)Glc3**Glc**3

Supplementary Figures

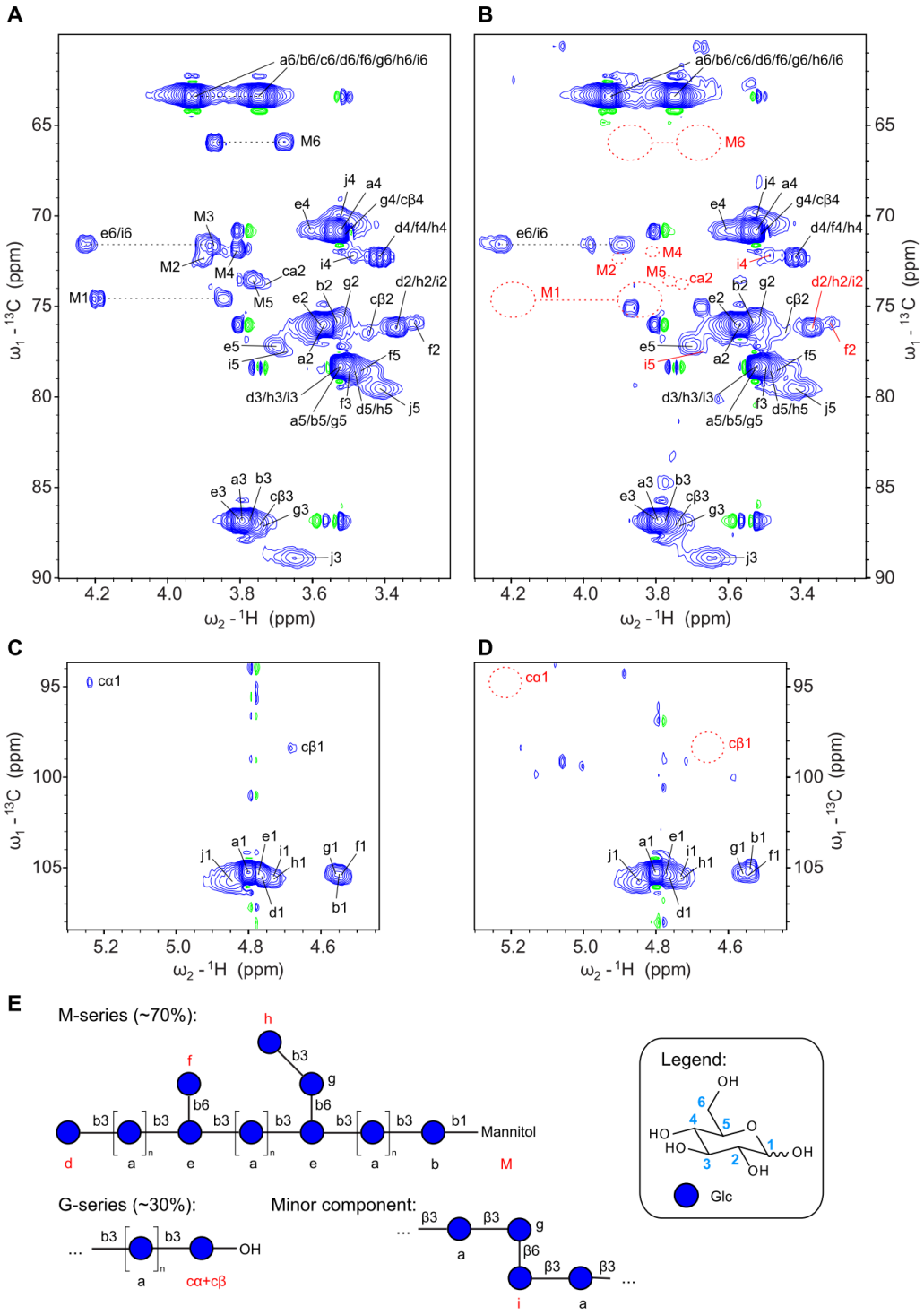

Supplementary Figure 1. Two-dimensional ^{1}H-^{13}C HSQC NMR spectra of untreated laminarin (A and C) and oxidized laminarin (B and D) with schematic structures (E). Panel A and C show the aliphatic region in which each ^{1}H-^{13}C one-bond correlation gives one signal (carbon C2 to C5) and methylene groups give two signals (H6-C6 and H6'-C6 connected by a dotted line). Positive signals are in blue, negative signals in green (only noise, artefacts and antiphase relay signals). Spin systems are labeled with a one-letter code and the number indicates the corresponding carbon. Spin systems in red indicate moieties whose signals either disappear or show reduced signal intensity upon periodate oxidation.

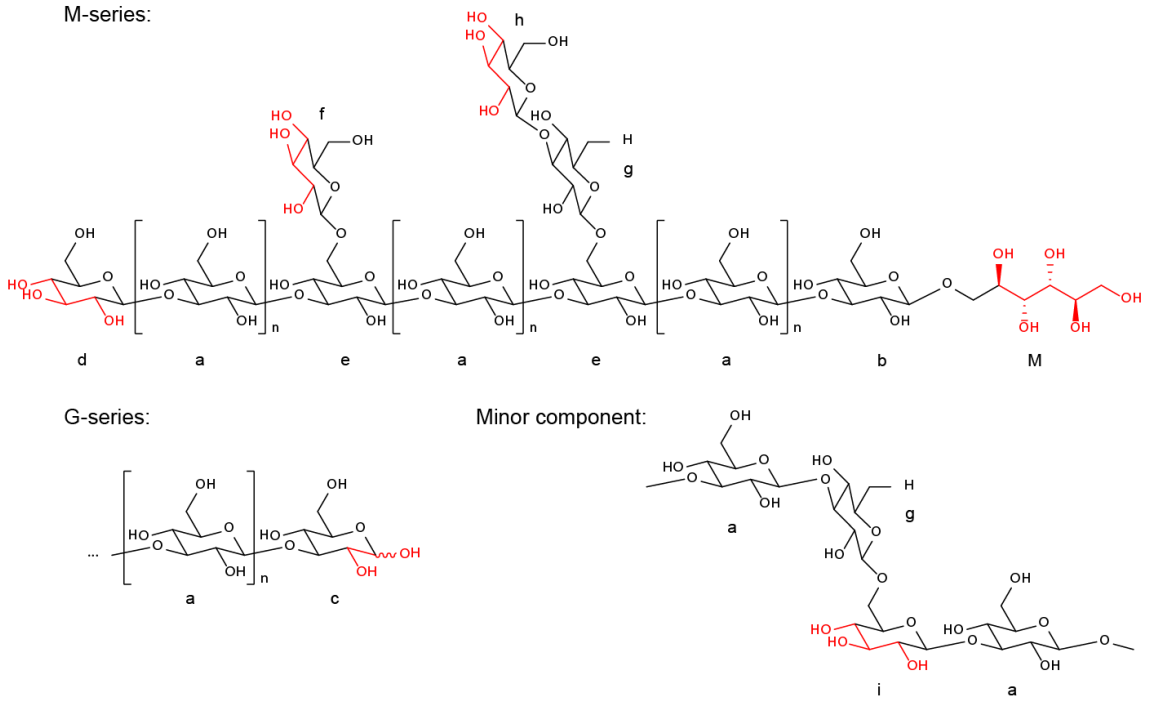

Supplementary Figure 2. Structure of laminarin as determined by NMR. Laminarin is heterogeneous and consists of a mixture of M-series and G-series molecules that end with mannitol (M) or an unprotected glucose (c) at the reducing end, respectively. Molecules vary in length and branching with an average number of 25 glucose moieties. Expected sites for periodate oxidation containing accessible, neighboring OH-groups (vicinal diols) are indicated in red.

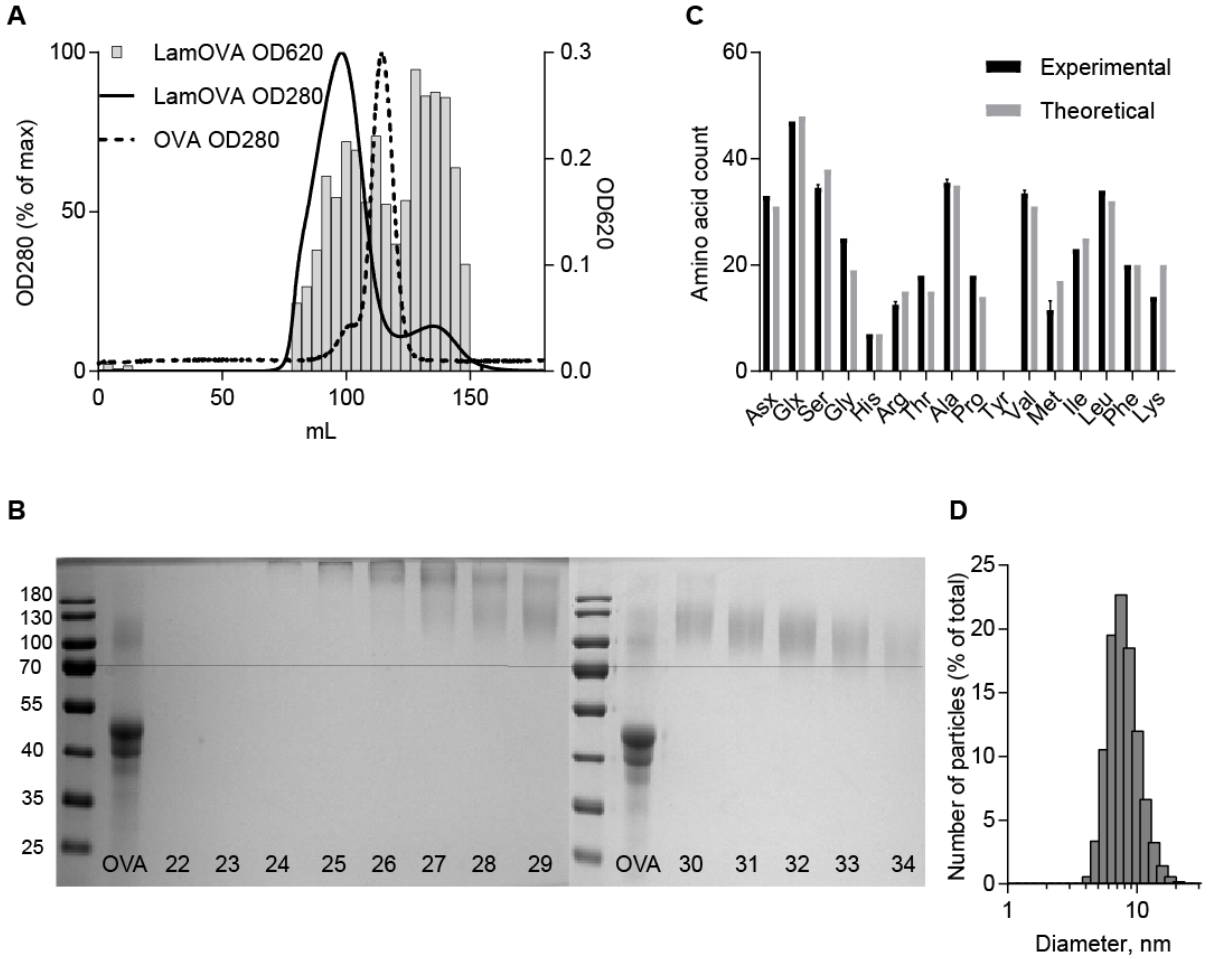

Supplementary Figure 3. Characterization of laminarin OVA conjugates. A) SEC chromatograms for LamOVA and OVA at 280nm. Laminarin concentration in LamOVA fractions was determined by anthrone method (620nm). B) OVA and LamOVA fractions 22-34 were analyzed by 10% SDS-PAGE and coomassie staining. Fractions 24-34 (elution between 70 and 100mL) migrated above 70kDa (threshold indicated by line) and were pooled for further analysis. C) Amino acid analysis. After reductive amination, only 14 of 20 lysine residues were detected. D) LamOVA size distribution (number-weighted) of particles as measured by dynamic light scattering. Mean hydrodynamic diameter was 8.27nm.

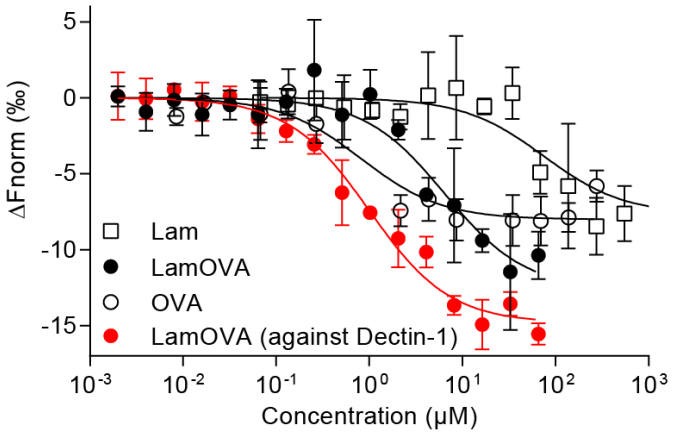

Supplementary Figure 4. Binding of soluble TLR5 receptor (fused to IgG-Fc) to soluble LamOVA, OVA, and laminarin. Data are shown as changes in normalized fluorescence (ΔFnorm) of MST measurements (mean±SD of three independent binding experiments). Binding of LamOVA to soluble Dectin-1 receptor is shown in red for reference.

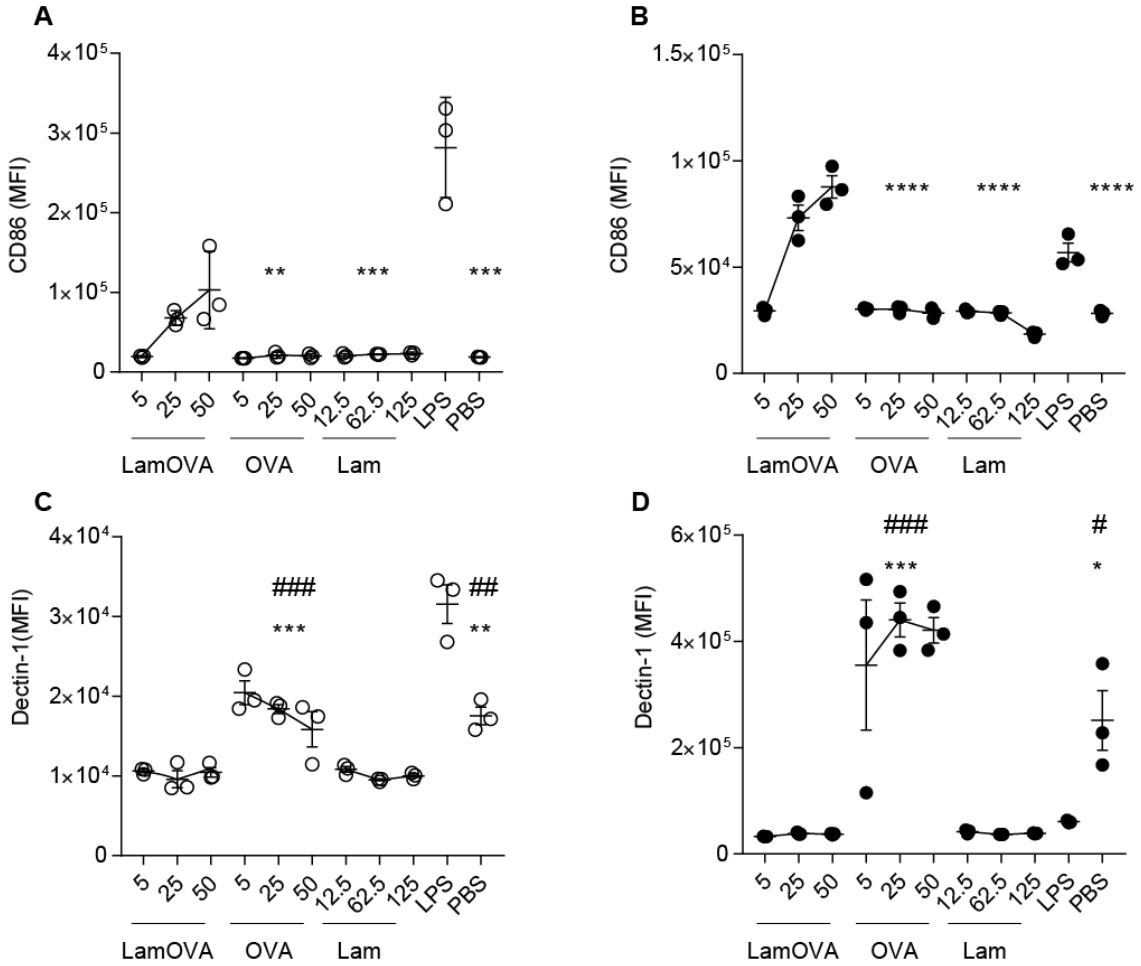

Supplementary Figure 5. CD86 and dectin-1 expression on stimulated BMDCs. GM- and FL-BMDCs were stimulated with LamOVA, OVA, or PBS for 24 hours. Protein concentrations for OVA and LamOVA were 5, 25, and 50µg/mL. Laminarin was used at equivalent doses as those present in LamOVA (12.5, 25, 62.5µg/mL). LPS (1µg/mL) served as positive control. Data are shown as median fluorescence intensity (MFI) of CD86 (A and B) and dectin-1 (C and D) on GM-BMDCs (A and C, white circles) and FL-BMDCs (B and D, black dots). Data are shown as means±SEM and individual replicates (n=3). Statistical significance vs. LamOVA (*), vs. OVA (#), and vs. PBS (§) was analyzed by two-way RM ANOVA followed by Tukey's multiple comparisons test.

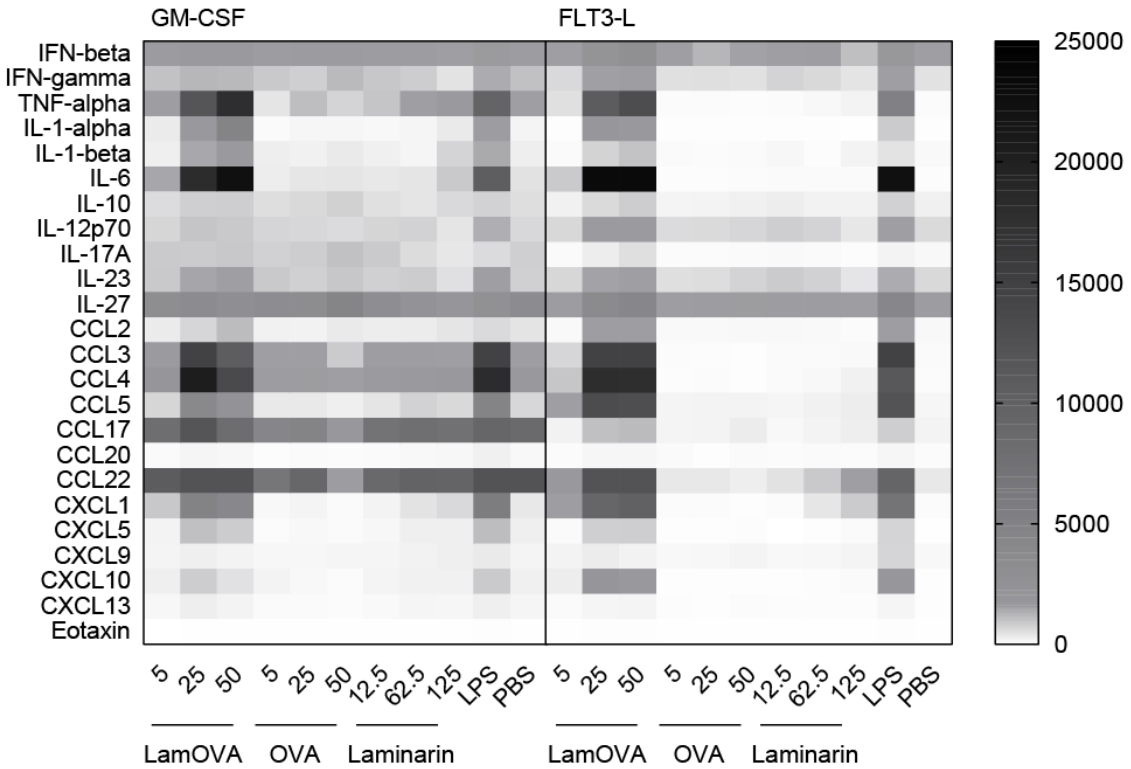

Supplementary Figure 6. Cytokine and chemokine secretion from stimulated BMDCs. GM- and FL-BMDCs were incubated 24h in the presence or absence of increasing doses of OVA, LamOVA or laminarin (shown in µg/mL). Laminarin was used at the same doses as present in LamOVA conjugates. 1 µg/mL LPS served as positive control. Data are shown as pg/mL.

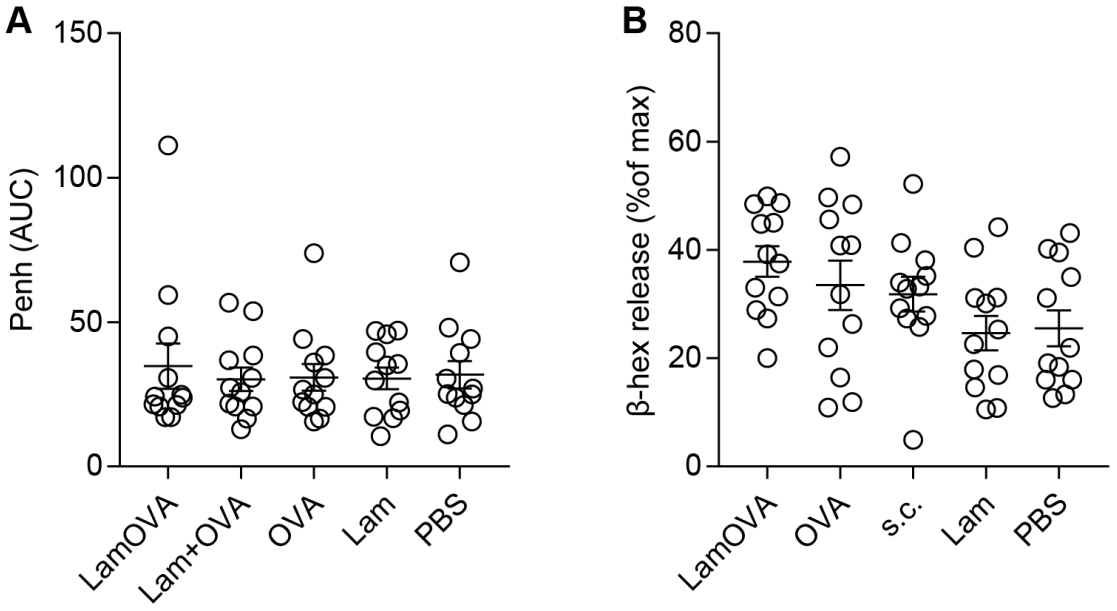

Supplementary Figure 7. Group stratification of sensitized mice before treatment. BALB/c mice were sensitized by two i.p. injections of OVA followed by two i.n challenges. A) Before treatment, airway hyperresponsiveness was assessed by WBP and mice were stratified into treatment groups with similar means and distribution of Penh. Data are shown as area under the curve (AUC) of a methacholine challenge dose response curve. B) Presence of OVA-specific IgE before treatment was confirmed by RBL assay (serum dilution 1:100). Data are shown as percentage of total beta-hexosaminidase release.

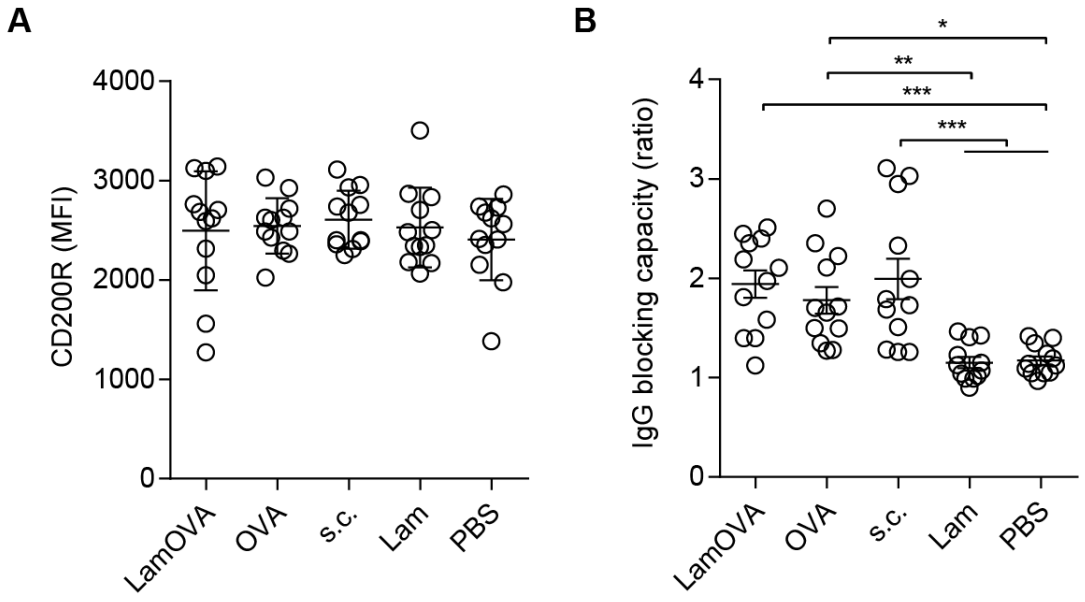

Supplementary Figure 8. Cell bound IgE and IgG blocking capacity after treatment and challenge. A) After the second aerosol challenge, blood was drawn and serum was washed away. After 2h *in vitro* restimulation with OVA, basophil activation status was assessed by flow cytometry as upregulation of CD200R. MFI = median fluorescence intensity. B) IgG blocking capacity is shown as the ratio of CD200R expression in basophils in the absence and presence of autologous serum. Data are shown as means±SEM and individual animals (n=12).

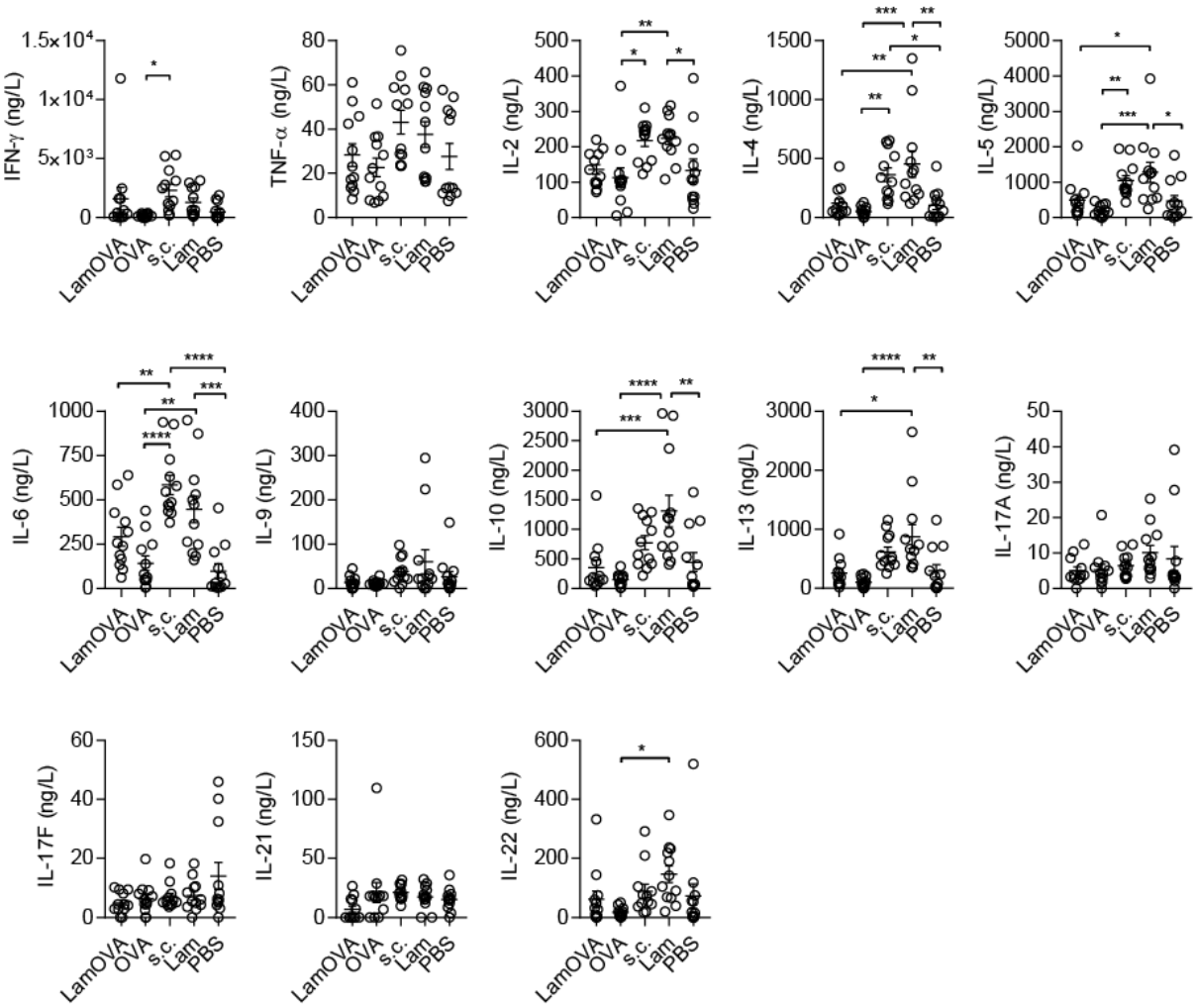

Supplementary Figure 9. Cytokine secretion of splenocytes restimulated with OVA for 3 days. Concentrations of different cytokines in cell culture supernatants was analyzed by flow cytometry using LEGENDplex assay. Data are shown as means±SEM and individual animals (n=12).

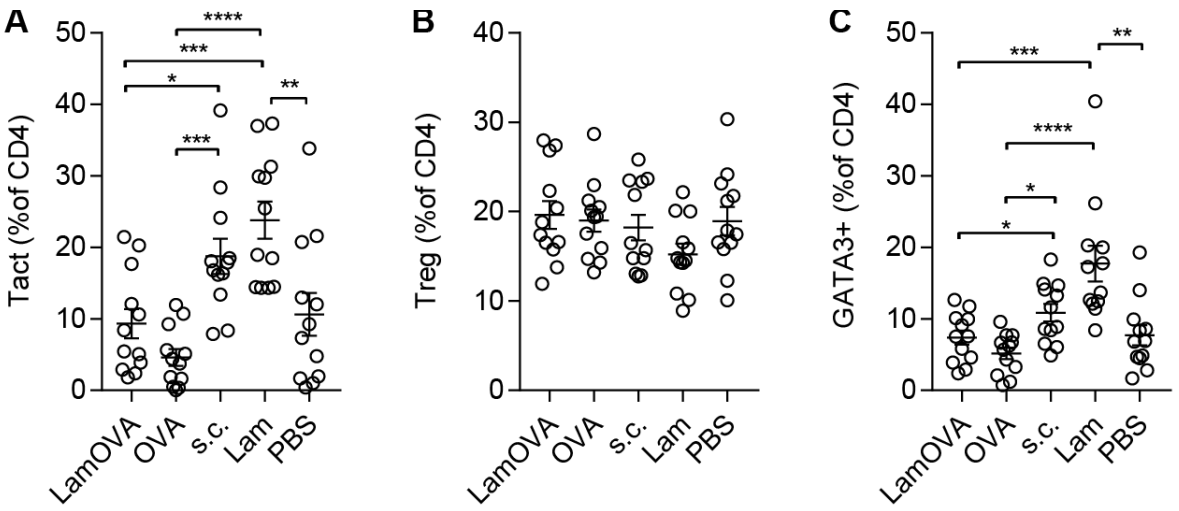

Supplementary Figure 10. Percentage of activated (Tact), regulatory (Treg) and GATA3+ T cells. Splenocytes were restimulated with OVA for 3 days and the percentage of Tact, Treg, and GATA3+ cell was assessed by flow cytometry. Data are shown as means±SEM and individual data points (n=12).

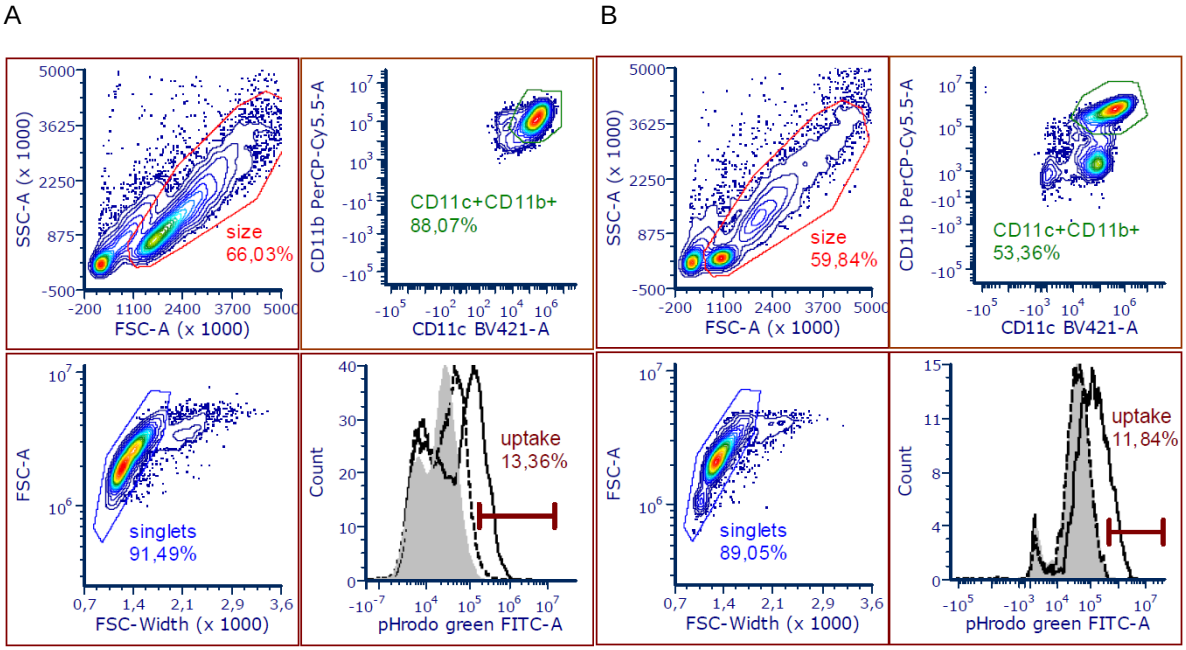

Supplementary Figure 11. Gating strategy for BMDCs. GM-BMDC (A) or FL-BMDCs (B) were first gated according to size to remove debris. Then, CD11c+CD11b+ cells were gated following exclusion of doublets on a FSC-W/FSC-A plot. The gated cells were then further analyzed for antigen uptake or expression of CD86 or dectin-1. Representative density plots and histograms from an uptake experiment are shown. Grey histogram shows PBS control, dotted line indicates cells incubated with pHrodo-OVA and solid line cells incubated with pHrodo-LamOVA.

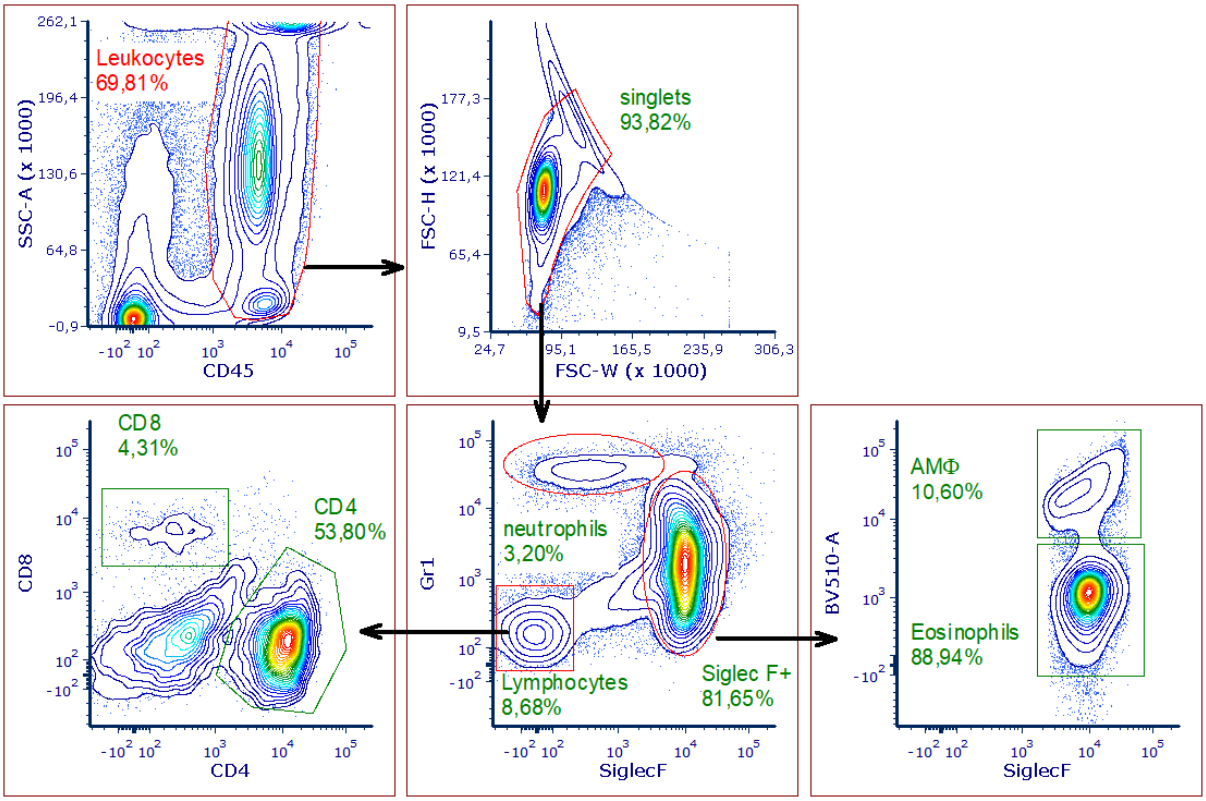

Supplementary Figure 12. Gating strategy for BAL Leukocytes. Total Leukocytes were gated based upon expression of CD45 followed by doublet exclusion. Neutrophils and lymphocytes were gated on a Siglec-F vs. Gr-1 plot. SiglecF+ cells were discriminated into alveolar macrophages (AMΦ) and eosinophils based on autofluorescence on the BV510 channel. Lymphocytes were further distributed into CD4+ and CD8+ cells.

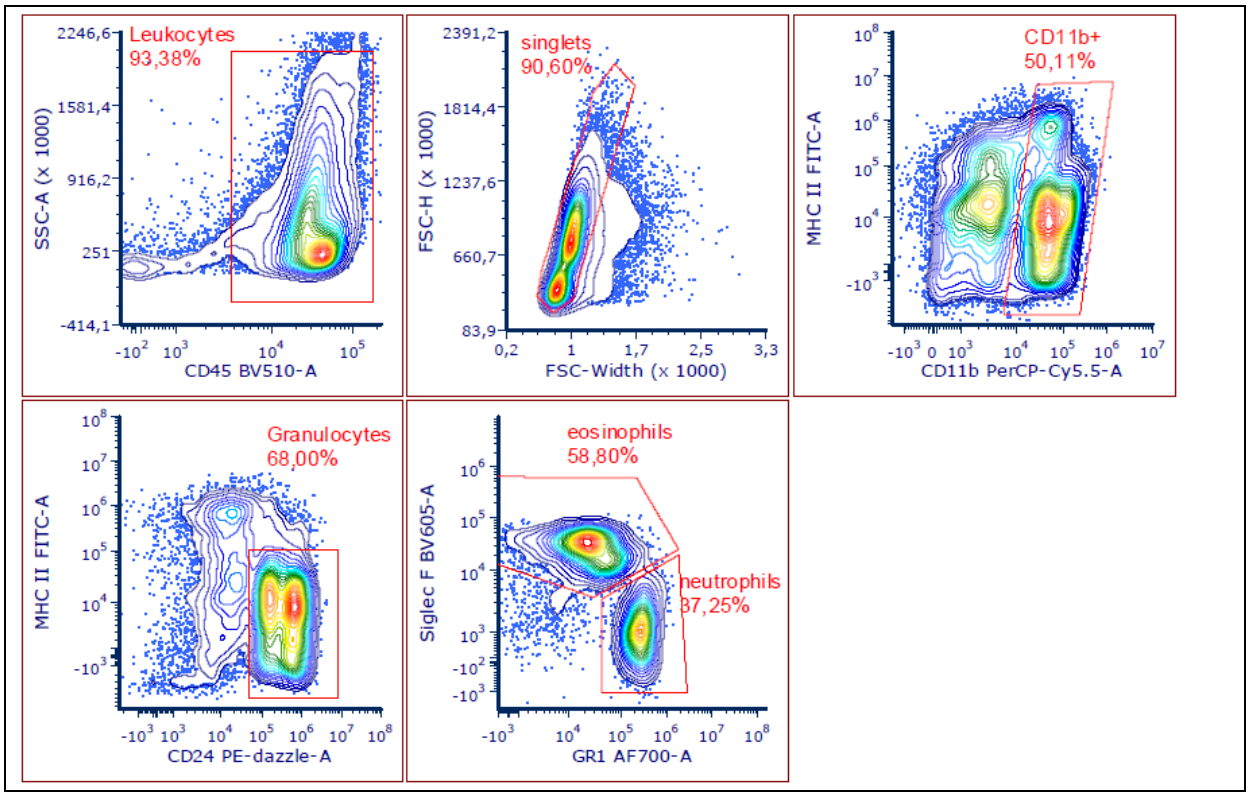

Supplementary Figure 13. Gating strategy lung digests. Total Leukocytes were gated based upon expression of CD45 followed by doublet exclusion. CD11b+ cells were gated on a MHC-II vs. CD11b plot. Granulocytes were identified as CD24+ MHC-II- cells and further separated into eosinophils and neutrophils based on SiglecF and Gr-1 expression.

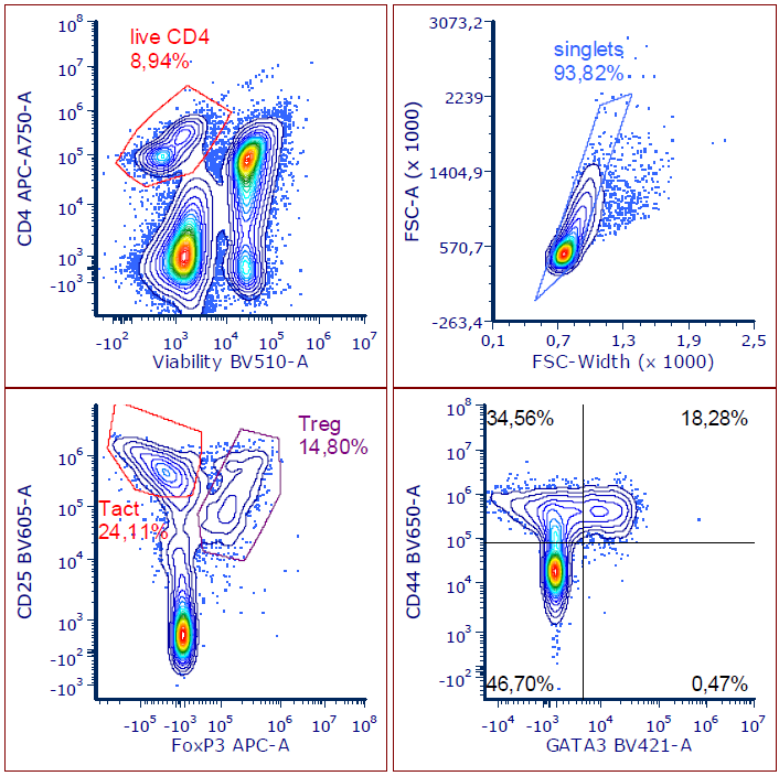

Supplementary Figure 14. Gating strategy splenocyte cultures. After in vitro restimulation, live CD4 cells were gated followed by doublet exclusion. Activated T cells (Tact) and regulatory T cells (Treg) were gated based on their expression of CD25 and FoxP3. Th2 cells were identified as CD44+GATA3+.

References

1. Markley JL, Bax A, Arata Y, et al. Recommendations for the presentation of NMR structures of proteins and nucleic acids. IUPAC-IUBMB-IUPAB Inter-Union Task Group on the Standardization of Data Bases of Protein and Nucleic Acid Structures Determined by NMR Spectroscopy. *J Biomol NMR.* 1998;12(1):1-23.
2. Gabler M, Scheiblhofer S, Kern K, et al. Immunization with a low-dose replicon DNA vaccine encoding Phl p 5 effectively prevents allergic sensitization. *J Allergy Clin Immunol.* 2006;118(3):734-741.
3. Misharin AV, Morales-Nebreda L, Mutlu GM, Budinger GR, Perlman H. Flow cytometric analysis of macrophages and dendritic cell subsets in the mouse lung. *Am J Respir Cell Mol Biol.* 2013;49(4):503-510.
4. Torrero MN, Larson D, Hubner MP, Mitre E. CD200R surface expression as a marker of murine basophil activation. *Clin Exp Allergy.* 2009;39(3):361-369.